

This figure "fig1a.jpg" is available in "jpg" format from:

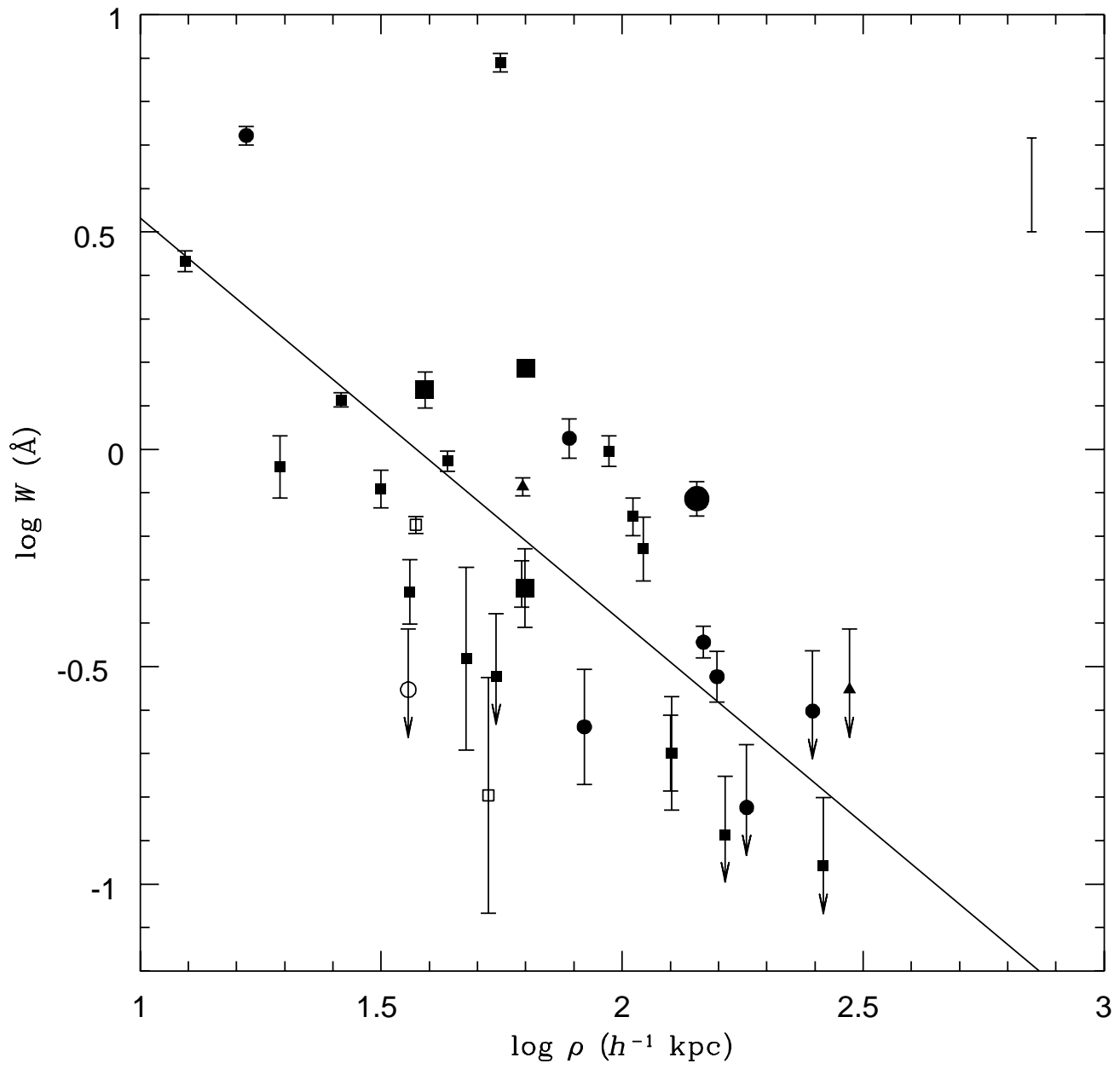
<http://arxiv.org/ps/astro-ph/9710310v2>

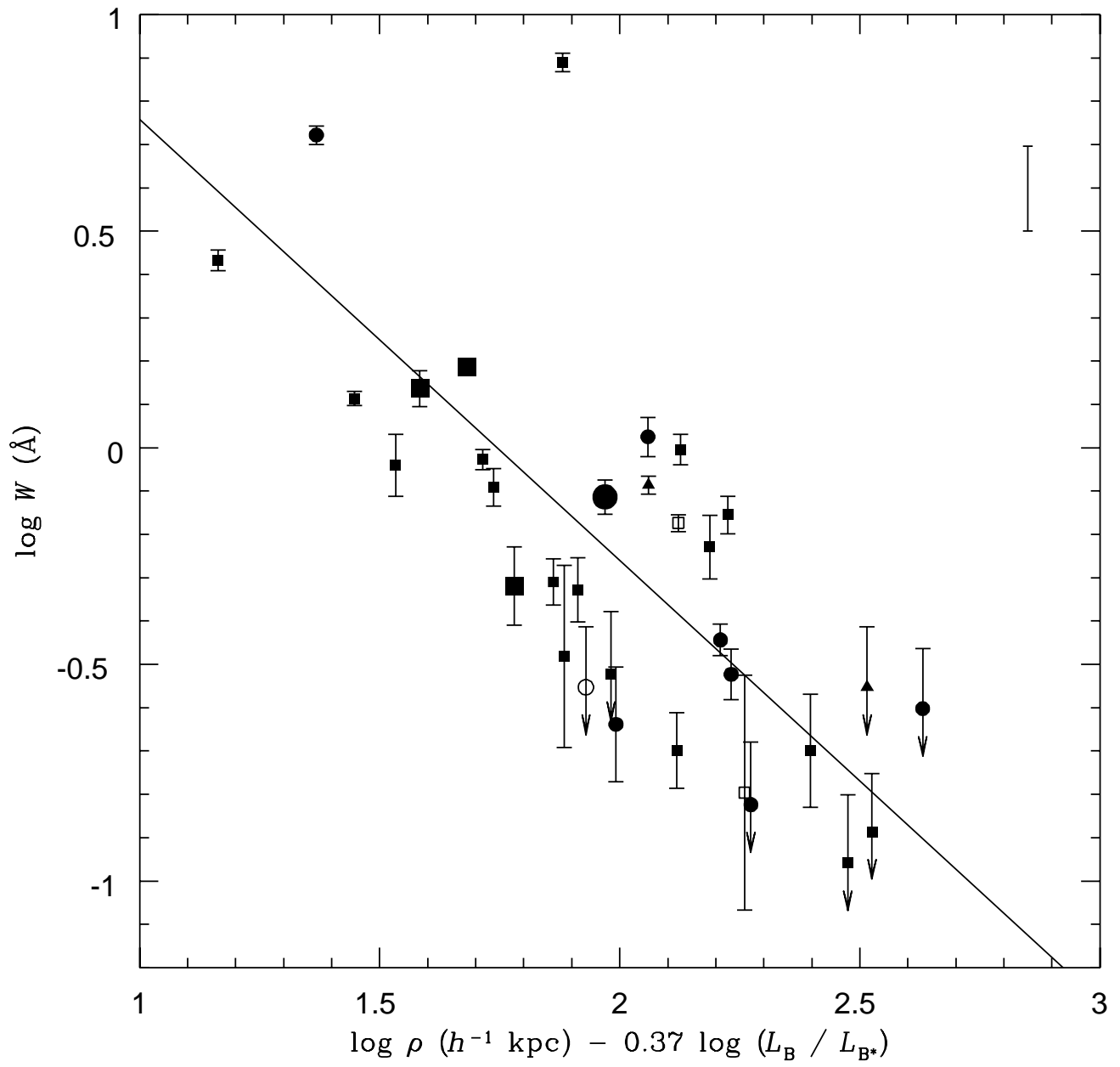
This figure "fig1b.jpg" is available in "jpg" format from:

<http://arxiv.org/ps/astro-ph/9710310v2>

This figure "fig1c.jpg" is available in "jpg" format from:

<http://arxiv.org/ps/astro-ph/9710310v2>





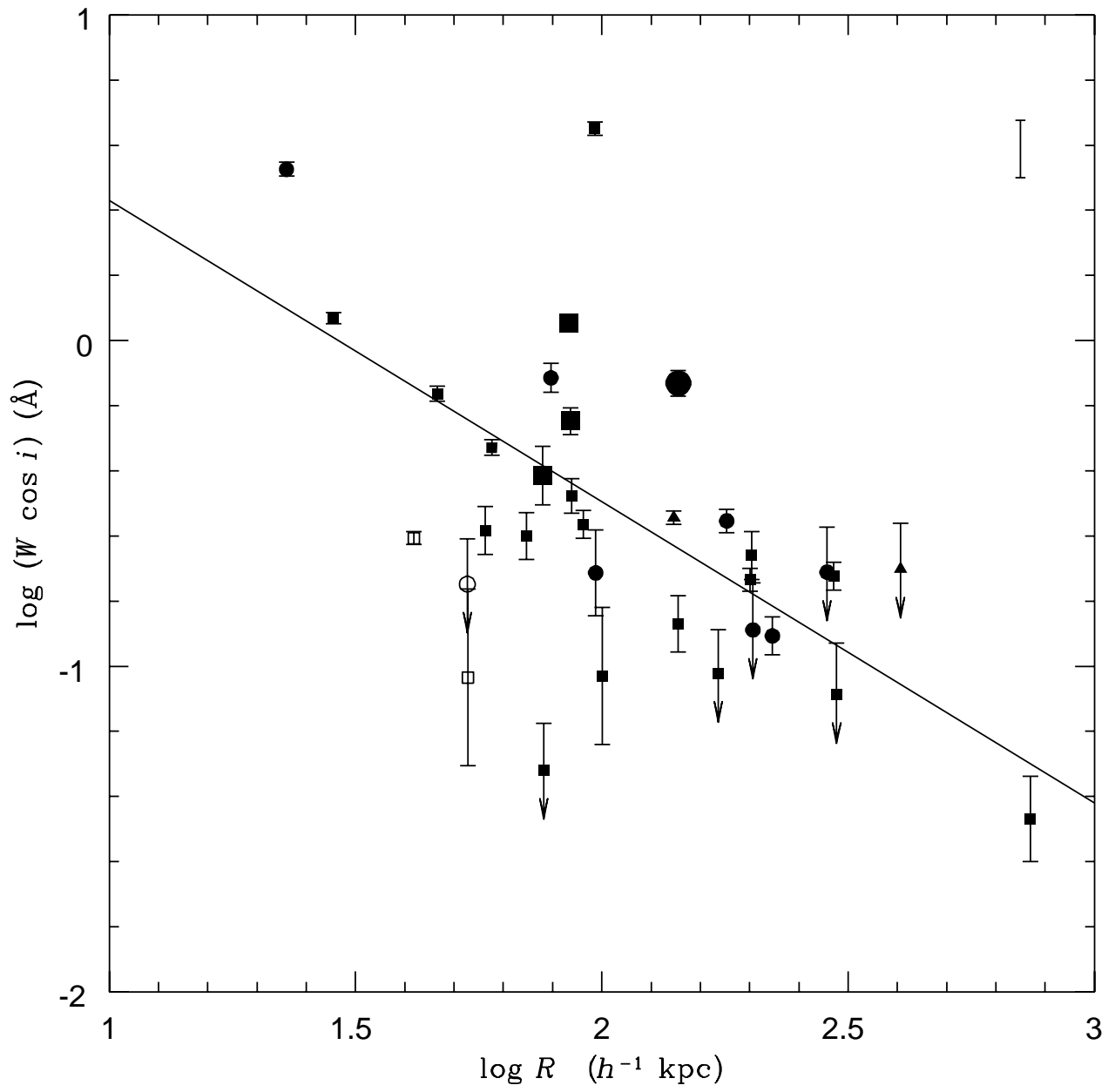


TABLE 4  
GALAXIES AND ABSORPTION SYSTEMS

Field	Galaxies											Absorption Systems			
	$\Delta\alpha$ (arcsec)	$\Delta\delta$ (arcsec)	$z_{\text{gal}}$	$\rho$ ( $h^{-1}$ kpc)	$R_D$ ( $h^{-1}$ kpc)	$R_B$ ( $h^{-1}$ kpc)	$D/B$	$\alpha$ (deg)	$i$ (deg)	$b/a$	$m$	$\langle\mu\rangle$	$M_B - 5 \log h$	$z_{\text{abs}}$	$W(\text{Ly}\alpha)$ ( $\text{\AA}$ )
0349-1438 .....	-9.4	10.8	0.3567	43.4	2.4	0.9	> 50	23.8	43.1	0.13	20.6	22.9	-19.0	0.3566	0.94
	11.7	-24.1	0.3236	77.0	2.8	1.2	0.4	170.6	83.0	0.39	20.0	24.7	-18.9	...	...
	-29.2	18.3	0.3244	99.1	...	1.2	0.0	100.8	...	0.74	19.5	22.5	-19.5	...	...
	12.6	-45.9	0.2617	120.3	1.8	0.4	1.6	35.2	58.1	0.96	20.2	24.4	-18.2	...	...
	-57.1	19.8	0.3273	174.7	3.1	...	> 50	170.1	57.6	...	20.2	23.0	-19.2	...	...
0405-1219 .....	10.6	-6.7	0.5714	46.9	...	5.4	0.0	75.9	80.5	0.81	20.5	25.0	-20.2	...	< 0.05
	-3.3	-12.7	0.5696	49.0	...	...	...	...	...	...	...	...	...	...	< 0.06
	2.6	-15.0	0.5657	56.8	...	2.0	0.0	71.7	...	0.81	20.8	23.0	-19.9	...	< 0.06
	10.4	-26.9	0.5779	108.3	...	2.7	0.0	43.3	...	0.83	21.0	23.8	-19.8	...	< 0.06
	1.0	-35.0	0.3520	105.4	1.6	...	> 50	47.4	74.3	...	21.5	22.3	-18.1	0.3514	0.70
	14.0	-35.4	0.5777	143.0	0.2	1.5	0.0	84.4	83.9	0.28	21.5	22.4	-19.4	...	< 0.06
	-37.2	28.4	0.3617	142.8	...	5.0	0.0	171.9	...	0.96	18.5	24.0	-20.8	0.3610	0.77
	16.1	-45.1	0.6167	183.9	3.4	...	> 50	0.8	61.1	...	21.6	22.8	-19.5	...	...
	-36.9	35.4	0.5696	191.1	4.4	2.1	1.4	59.1	73.1	0.72	20.6	24.3	-20.2	...	< 0.06
	31.9	-47.9	0.2973	157.4	3.6	3.9	1.2	153.2	39.8	0.41	19.5	25.6	-19.3	0.2980	0.30
	19.2	-70.0	0.5170	261.6	3.4	0.5	> 50	141.3	41.8	0.20	21.5	24.4	-19.1	...	< 0.11
	-66.2	-30.9	0.1525	126.3	5.4	0.3	> 50	29.2	47.5	0.85	18.3	25.2	-19.4	0.1532	0.20
	-65.6	56.7	0.2800	228.7	...	...	...	...	...	...	...	...	...	...	< 0.13
0454-2203 .....	10.6	5.7	0.2784	31.6	3.4	0.1	> 50	77.5	70.3	0.91	21.1	24.1	-17.9	0.2777	0.81
	-1.1	-18.0	0.4847	63.3	7.1	0.3	> 50	96.2	42.6	0.79	20.1	24.3	-20.3	0.4825	1.54
	4.2	18.4	0.5325	68.8	...	1.0	0.0	135.7	...	0.43	21.8	22.6	-18.7	...	< 0.04
	0.3	-19.7	0.3818	61.9	1.6	0.1	> 50	65.7	47.2	0.62	20.8	22.2	-19.0	0.3812	0.49
	-18.2	42.9	0.4836	163.4	6.0	0.6	7.4	151.7	70.5	0.82	20.4	25.4	-20.0	...	...
	37.8	-36.5	0.4837	184.3	3.8	0.2	> 50	5.5	31.6	0.85	20.1	23.4	-20.4	...	...
	35.6	-41.0	0.5336	198.1	7.3	1.4	> 50	50.1	75.7	0.54	21.0	23.6	-19.6	...	< 0.04
0850+4400 .....	14.5	99.5	0.3382	296.1	1.6	0.2	10.0	69.5	44.7	0.82	20.2	23.0	-19.2	...	< 0.28
	-8.9	2.0	0.1635	16.6	1.4	2.5	0.4	51.7	55.9	0.64	18.7	25.4	-18.5	0.1630	5.27
	10.0	-2.4	0.4402	34.6	5.0	1.8	0.6	161.2	10.7	0.66	20.6	24.9	-19.3	...	< 0.23
	22.6	12.4	0.5007	91.7	3.2	0.1	> 50	165.7	61.0	0.86	20.9	24.5	-19.6	...	< 0.08
	3.4	35.0	0.0872	38.5	...	1.3	0.0	145.1	...	0.94	17.4	23.7	-18.3	...	...
	-0.5	40.5	0.0915	46.2	1.8	...	> 50	30.0	74.5	...	19.9	24.4	-16.6	...	...
	29.0	30.5	0.2766	110.2	2.5	...	> 50	123.3	11.6	...	20.9	24.2	-18.1	...	...
1001+2910 .....	45.5	2.2	0.5196	164.5	...	2.4	0.0	93.8	...	0.88	20.1	23.0	-20.4	...	< 0.09
	-3.4	-23.1	0.1380	37.6	1.8	...	> 50	11.2	68.3	...	21.7	24.9	-15.7	0.1377	0.67
	-28.4	6.6	0.3308	85.0	1.1	1.0	0.9	83.4	66.6	0.79	20.5	23.1	-18.5	0.3285	0.18

TABLE 4 *continued*

Field	Galaxies											Absorption Systems			
	$\Delta\alpha$ (arcsec)	$\Delta\delta$ (arcsec)	$z_{\text{gal}}$	$\rho$ ( $h^{-1}$ kpc)	$R_D$ ( $h^{-1}$ kpc)	$R_B$ ( $h^{-1}$ kpc)	$D/B$	$\alpha$ (deg)	$i$ (deg)	$b/a$	$m$	$\langle\mu\rangle$	$M_B - 5 \log h$	$z_{\text{abs}}$	$W(\text{Ly}\alpha)$ ( $\text{\AA}$ )
1354+1933 .....	1.2	7.5	0.4592	26.1	3.1	...	> 50	112.3	25.6	...	21.0	23.4	-19.3	0.4569	1.30
	-21.6	-12.2	0.4406	83.5	0.6	3.2	0.1	111.9	67.8	0.84	20.9	25.1	-19.0	0.4412	0.23
	-16.0	-23.3	0.4295	94.1	4.2	...	> 50	159.1	79.3	...	21.6	23.3	-18.5	0.4306	0.99
	-13.4	-48.0	0.5293	181.3	0.1	2.6	0.0	122.1	1.8	0.86	21.1	24.2	-19.4	...	< 0.15
	65.8	50.1	0.3509	248.5	1.0	6.5	0.5	134.7	73.2	0.78	21.3	22.5	-17.9	...	< 0.25
1545+2102 .....	-2.7	+1.1	0.2657	7.2	0.3	2.6	0.0	143.6	75.4	0.91	19.9	24.3	-19.0	0.2641	0.63
	16.6	-8.7	0.2639	47.6	2.8	2.1	2.2	18.8	20.6	0.80	19.5	23.5	-19.4	...	...
	-26.3	23.1	0.1343	55.1	4.2	...	> 50	9.0	80.8	...	19.7	23.6	-17.8	...	< 0.30
	27.3	-35.6	0.0949	53.4	1.8	...	> 50	6.6	54.7	...	20.9	24.9	-15.8	0.0961	0.16
1622+2352 .....	-1.5	2.1	0.9310	10.9	2.6	0.5	13.1	93.5	69.4	0.94	24.0	23.0	-18.7	0.8912	2.71
	3.0	-0.0	0.8920	12.4	4.2	0.8	28.6	124.1	80.0	0.54	23.3	26.7	-19.0	0.8909	2.71
	-4.2	-3.8	0.4720	19.5	1.3	...	> 50	96.8	74.0	...	22.5	22.4	-17.8	0.4716	0.91
	-5.5	7.5	0.6352	36.3	0.7	...	> 50	123.5	56.2	...	24.1	22.7	-17.1	0.6359	0.47
	-8.9	3.2	0.7980	39.0	3.8	...	> 50	63.6	65.6	...	22.4	22.8	-19.6	0.7964	1.37
	-3.3	9.1	0.5650	36.0	...	0.2	0.0	115.0	...	0.64	23.8	22.5	-17.0	0.5658	< 0.28
	-1.3	11.3	0.9210	47.9	0.4	4.0	0.0	12.1	64.3	0.43	22.2	23.5	-20.8	...	< 0.09
	-6.7	9.7	0.3180	33.6	2.6	3.3	0.9	58.6	72.0	0.75	20.2	26.4	-18.7	...	...
	-11.1	-4.3	1.0370	51.0	2.5	...	> 50	37.4	56.1	...	23.7	22.6	-19.3	...	...
	-5.1	11.1	0.9200	51.4	0.5	2.4	0.8	53.5	61.4	0.45	23.8	21.3	-19.3	...	< 0.09
	7.3	-12.1	0.9200	59.5	7.2	0.3	> 50	147.6	18.6	0.36	21.8	23.4	-20.7	...	< 0.09
	1.6	14.2	0.6560	55.9	3.1	0.2	> 50	87.7	54.7	0.42	22.7	23.6	-18.6	0.6564	7.75
	-12.3	9.9	0.7020	62.8	2.5	0.1	> 50	114.7	36.7	0.34	21.9	22.6	-19.6	0.7020	0.48
	18.2	0.2	1.0100	77.7	2.1	...	> 50	82.5	70.6	...	24.9	23.2	-17.9	...	...
	7.9	-17.0	0.8280	77.7	0.5	0.6	0.3	169.6	58.1	0.73	24.2	22.7	-18.4	0.8273	1.06
	-21.3	-6.2	0.3680	68.4	2.8	...	> 50	91.7	58.3	...	19.9	22.1	-19.8	...	...
	-24.1	5.3	0.3680	75.9	1.2	...	> 50	96.5	74.7	...	23.4	23.7	-16.3	...	...
	15.0	19.6	1.0180	105.2	...	...	...	...	...	...	...	...	...	...	...
	8.8	-24.8	0.9190	111.0	2.6	...	> 50	130.6	51.3	...	22.4	22.9	-20.1	...	< 0.09
	-26.4	-2.7	0.9240	111.8	0.3	2.4	0.0	33.1	61.5	0.85	22.7	23.2	-20.4	...	< 0.08
	-28.9	5.7	0.9230	124.1	1.5	...	> 50	172.5	60.5	...	24.3	22.7	-18.2	...	< 0.09
	25.5	17.6	0.2610	78.1	1.6	1.0	4.8	48.2	56.2	0.47	21.6	25.1	-17.2	...	...
	-7.9	30.7	0.7090	126.7	2.2	...	> 50	95.9	80.2	...	24.0	23.4	-17.5	0.7090	0.20
	12.7	-31.2	0.2800	88.9	0.3	0.5	0.0	112.4	84.7	0.63	22.9	26.0	-15.7	...	...
	-34.3	3.2	1.0110	146.9	...	...	...	...	...	...	...	...	...	...	...
	-7.6	-43.4	0.8920	184.6	2.0	...	> 50	5.6	31.5	...	23.8	23.2	-18.6	...	...
	-45.4	7.7	0.6680	181.1	2.1	...	> 50	13.4	65.3	...	24.4	24.4	-16.9	...	...
	-46.8	7.7	0.6380	183.9	3.6	...	> 50	0.6	81.8	...	24.9	24.7	-16.3	...	...



TABLE 4 *continued*

Field	Galaxies												Absorption Systems		
	$\Delta\alpha$ (arcsec)	$\Delta\delta$ (arcsec)	$z_{\text{gal}}$	$\rho$ ( $h^{-1}$ kpc)	$R_D$ ( $h^{-1}$ kpc)	$R_B$ ( $h^{-1}$ kpc)	$D/B$	$\alpha$ (deg)	$i$ (deg)	$b/a$	$m$	$\langle\mu\rangle$	$M_B - 5 \log h$	$z_{\text{abs}}$	$W(\text{Ly}\alpha)$ ( $\text{\AA}$ )
1704+6048 .....	8.1	-27.1	0.3615	86.4	2.9	...	> 50	129.5	61.3	...	20.6	22.8	-19.1	0.3621	0.49
	-31.3	-9.4	0.3380	96.2	3.2	...	> 50	136.7	58.6	...	21.5	24.2	-18.0	...	...
	-14.2	-30.4	0.0713	30.8	0.7	...	> 50	133.1	78.9	...	21.8	24.0	-14.1	...	...
	26.8	-35.2	0.3731	136.9	...	3.3	0.0	92.8	...	0.63	19.6	23.7	-19.8	0.3716	0.26
	-51.0	18.3	0.0921	62.2	3.7	0.7	9.9	131.4	69.6	0.93	18.7	26.7	-17.7	0.0920	0.82
	54.4	10.2	0.4033	178.7	1.9	...	> 50	11.2	60.8	...	21.5	22.8	-18.4	...	...
	-70.0	13.3	0.2260	163.6	2.5	0.1	> 50	20.7	43.0	0.58	21.2	24.6	-17.4	...	< 0.13
	72.9	5.9	0.1877	147.4	0.4	2.9	0.0	121.7	89.8	0.78	18.3	24.3	-19.2	0.1880	0.36
	2135-1446 .....	4.7	-2.6	0.1996	11.3	2.5	1.5	1.0	88.6	78.7	0.66	19.7	24.8	-18.5	0.2005
-7.3		15.7	0.2000	36.6	...	1.3	0.0	143.7	...	0.48	19.2	22.6	-19.0	...	...
13.1		-21.7	0.1986	53.3	1.6	1.3	> 50	63.0	54.7	0.01	20.5	24.3	-18.0	...	...
18.6		-33.5	0.1991	80.8	2.5	1.4	4.4	25.5	39.5	0.39	20.0	24.4	-18.4	...	...
28.4		-31.3	0.2011	89.6	2.8	...	> 50	157.7	54.3	...	18.3	22.6	-20.2	...	...
-0.8		49.3	0.0752	47.8	4.6	...	> 50	146.8	73.6	...	18.2	24.0	-18.1	0.0750	0.33
50.8		-21.7	0.1857	111.0	2.1	0.1	> 50	142.5	68.2	0.66	19.8	22.5	-18.5	0.1861	0.59

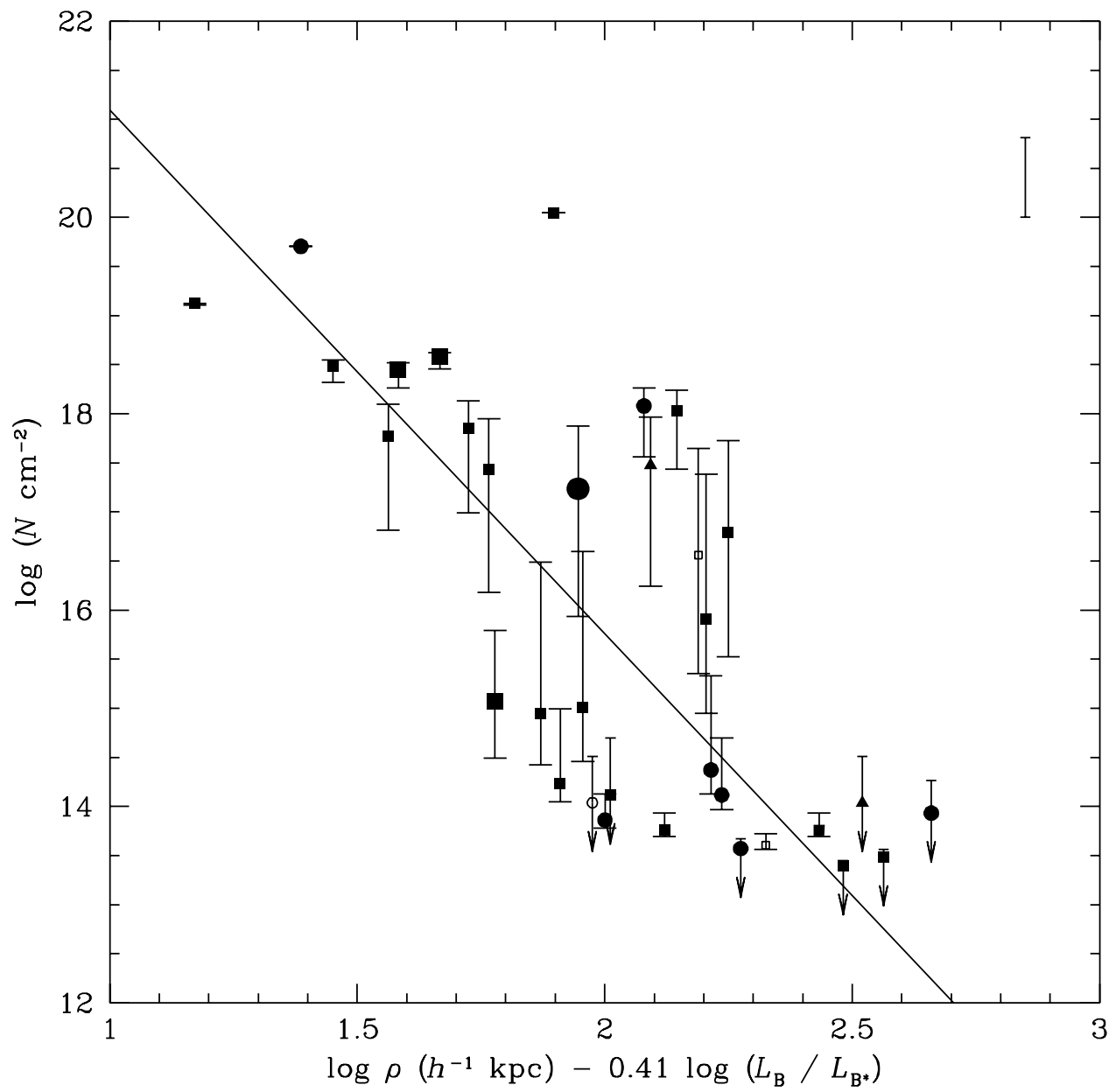


TABLE 5  
RESULTS OF STATISTICAL TESTS

Measurements	$a/\delta a$	Generalized		Kendall		Spearman		Pearson		$\sigma_c$
		Kendall		Kendall		Spearman		Pearson		
		$r_{gk}$	$r_{gk}/\sigma_{gk}$	$r_k$	$r_k/\sigma_k$	$r_s$	$r_s/\sigma_s$	$r_p$	$r_p/\sigma_p$	
1. $W - \rho$	7.2	-0.43	-3.54	-0.42	-3.47	-0.59	-3.36	-0.63	-4.45	0.217
2. $W - \rho - L_B$	8.5,3.6	-0.57	-4.71	-0.57	-4.68	-0.75	-4.26	-0.73	-5.79	0.197
3. $W - \rho - r_e$	8.8,3.7	-0.48	-3.95	-0.47	-3.87	-0.67	-3.77	-0.66	-4.82	0.210
4. $W - \rho - \langle \mu \rangle$	7.1,0.3	-0.45	-3.70	-0.44	-3.63	-0.61	-3.45	-0.63	-4.44	0.225
5. $W - \rho - D/B$	7.2,0.0	-0.43	-3.54	-0.42	-3.47	-0.59	-3.36	-0.63	-4.45	0.217
6. $W - \rho - (1+z)$	7.9,3.2	-0.48	-4.02	-0.48	-3.97	-0.68	-3.83	-0.65	-4.73	0.214
7. $W - R$	5.4	-0.33	-2.71	-0.33	-2.70	-0.48	-2.69	-0.50	-3.15	0.239
8. $W \cos i - R$	9.7	-0.37	-3.08	-0.34	-2.82	-0.48	-2.73	-0.54	-3.55	0.177
9. $W \cos i - R - L_B$	11.4,5.8	-0.55	-4.59	-0.52	-4.28	-0.71	-4.04	-0.71	-5.50	0.141
10. $W \cos i - R - r_e$	11.1,4.1	-0.38	-3.22	-0.34	-2.82	-0.48	-2.71	-0.56	-3.69	0.153
11. $W \cos i - R - \langle \mu \rangle$	10.1,0.1	-0.37	-3.07	-0.34	-2.82	-0.48	-2.74	-0.54	-3.56	0.167
12. $W \cos i - R - D/B$	9.4,0.3	-0.36	-3.00	-0.34	-2.76	-0.48	-2.72	-0.55	-3.59	0.187
13. $W \cos i - R - (1+z)$	8.5,1.3	-0.43	-3.61	-0.41	-3.35	-0.60	-3.38	-0.60	-4.15	0.233
14. $N - \rho$	9.9	-0.43	-3.57	-0.43	-3.50	-0.60	-3.38	-0.61	-4.25	1.050
15. $N - \rho - L_B$	10.7,4.0	-0.57	-4.77	-0.58	-4.71	-0.76	-4.27	-0.71	-5.58	0.815
16. $N - \rho - r_e$	9.9,3.2	-0.49	-4.11	-0.49	-4.03	-0.68	-3.86	-0.65	-4.73	0.939
17. $N - \rho - \langle \mu \rangle$	8.7,0.6	-0.45	-3.70	-0.44	-3.63	-0.61	-3.45	-0.61	-4.24	1.084
18. $N - \rho - D/B$	10.4,1.2	-0.44	-3.67	-0.44	-3.56	-0.61	-3.47	-0.61	-4.26	1.115
19. $N - \rho - (1+z)$	11.1,4.1	-0.50	-4.14	-0.50	-4.06	-0.67	-3.81	-0.64	-4.61	1.240
20. $N - R$	9.0	-0.34	-2.80	-0.34	-2.79	-0.48	-2.74	-0.48	-2.98	1.355
21. $N \cos i - R$	9.6	-0.33	-2.77	-0.33	-2.67	-0.46	-2.62	-0.50	-3.15	1.307
22. $N \cos i - R - L_B$	9.1,3.2	-0.46	-3.83	-0.45	-3.66	-0.61	-3.47	-0.60	-4.12	1.221
23. $N \cos i - R - r_e$	9.6,3.0	-0.36	-3.04	-0.34	-2.82	-0.49	-2.76	-0.54	-3.52	0.896
24. $N \cos i - R - \langle \mu \rangle$	8.4,0.1	-0.32	-2.66	-0.31	-2.57	-0.45	-2.54	-0.50	-3.16	1.352
25. $N \cos i - R - D/B$	8.7,1.7	-0.34	-2.84	-0.32	-2.60	-0.45	-2.54	-0.51	-3.25	1.401
26. $N \cos i - R - (1+z)$	11.8,5.2	-0.38	-3.19	-0.37	-3.04	-0.55	-3.14	-0.58	-3.91	1.023

**THE GASEOUS EXTENT OF GALAXIES AND THE ORIGIN OF  $\text{Ly}\alpha$   
ABSORPTION SYSTEMS. III. HUBBLE SPACE TELESCOPE IMAGING  
OF  $\text{Ly}\alpha$ -ABSORBING GALAXIES AT  $z < 1$ <sup>1</sup>**

HSIAO-WEN CHEN and KENNETH M. LANZETTA

Department of Physics and Astronomy, State University of New York at Stony Brook  
Stony Brook, NY 11794–3800, U.S.A.  
hchen,lanzetta@sbast3.ess.sunysb.edu

JOHN K. WEBB

School of Physics, University of New South Wales  
Sydney 2052, NSW, AUSTRALIA  
jkw@edwin.phys.unsw.edu.au

and

XAVIER BARCONS

Instituto de Física de Cantabria (Consejo Superior de Investigaciones Científicas—  
Universidad de Cantabria), Facultad de Ciencias  
39005 Santander, SPAIN

and

Institute of Astronomy, Madingley Road, Cambridge CB3 0HA, UK  
barcons@ifca.unican.es

---

<sup>1</sup>Based on observations with the NASA/ESA Hubble Space Telescope, obtained at the Space Telescope Science Institute, which is operated by the Association of Universities for Research in Astronomy, Inc., under NASA contract NAS5–26555.

## ABSTRACT

We present initial results of a program to obtain and analyze HST WFPC2 images of galaxies identified in an imaging and spectroscopic survey of faint galaxies in fields of HST spectroscopic target QSOs. We measure properties of 87 galaxies, of which 33 are associated with corresponding Ly $\alpha$  absorption systems and 24 do not produce corresponding Ly $\alpha$  absorption lines to within sensitive upper limits. Considering only galaxy and absorber pairs that are likely to be physically associated and excluding galaxy and absorber pairs within  $3000 \text{ km s}^{-1}$  of the background QSOs leaves 26 galaxy and absorber pairs and seven galaxies that do not produce corresponding Ly $\alpha$  absorption lines to within sensitive upper limits. Redshifts of the galaxy and absorber pairs range from 0.0750 to 0.8912 with a median of 0.3718, and impact parameter separations of the galaxy and absorber pairs range from 12.4 to  $157.4 h^{-1} \text{ kpc}$  with a median of  $62.4 h^{-1} \text{ kpc}$ . The primary result of the analysis is that the amount of gas encountered along the line of sight depends on the galaxy impact parameter and  $B$ -band luminosity but does not depend strongly on the galaxy average surface brightness, disk-to-bulge ratio, or redshift. This result confirms and improves upon the anti-correlation between Ly $\alpha$  absorption equivalent width and galaxy impact parameter found previously by Lanzetta et al. (1995). Spherical halos cannot be distinguished from flattened disks on the basis of the current observations, and there is no evidence that galaxy interactions play an important role in distributing tenuous gas around galaxies in most cases. Galaxies might account for all Ly $\alpha$  absorption systems with  $W > 0.3 \text{ \AA}$ , but this depends on the unknown luminosity function and gaseous cross sections of low-luminosity galaxies as well as on the uncertainties of the observed number density of Ly $\alpha$  absorption systems.

*Subject headings:* galaxies: evolution—quasars: absorption lines

## 1. INTRODUCTION

Although it is generally believed that low-redshift Ly $\alpha$  absorption systems are associated with galaxies and thus trace the large-scale structure of the universe, the existence of a physical connection between individual galaxies and individual Ly $\alpha$  absorption systems is still a matter of some debate (Morris et al. 1993; Lanzetta et al. 1995; Stocke et al. 1995; Bowen, Blades, & Pettini 1996; Le Brun, Bergeron, & Boissé 1996; van Gorkom et al. 1996). Over the past several years we have been conducting an imaging and spectroscopic survey of faint galaxies in fields of Hubble Space Telescope (HST) spectroscopic target QSOs (Lanzetta et al. 1995; Lanzetta, Webb, & Barcons 1995, 1996, 1997a,b; Barcons, Lanzetta, & Webb 1995). The goal of the survey is to establish the relationship between galaxies and Ly $\alpha$  absorption systems by directly comparing galaxies and Ly $\alpha$  absorption systems along common lines of sight. One of the most striking results of the survey is that there exists a distinct anti-correlation between Ly $\alpha$  absorption equivalent width and galaxy impact parameter. In particular, galaxies at impact parameters less than  $\approx 160 h^{-1}$  kpc are *almost always* associated with corresponding Ly $\alpha$  absorption lines, whereas galaxies at impact parameters greater than  $\approx 160 h^{-1}$  kpc are *almost never* associated with corresponding Ly $\alpha$  absorption lines. On the basis of this result, we conclude that most galaxies are surrounded by extended gaseous envelopes of  $\approx 160 h^{-1}$  kpc radius and that many or most Ly $\alpha$  absorption systems arise in extended gaseous envelopes of galaxies, where by “gaseous envelope” we mean simply a gaseous structure of large covering factor but unspecified geometry or filling factor.

But the scatter about the mean relationship between Ly $\alpha$  absorption equivalent width and galaxy impact parameter is substantial—specifically, the dispersion spans roughly a factor of two. Evidently the amount of gas encountered along the line of sight depends on other factors besides galaxy impact parameter, including perhaps galaxy luminosity, size, or morphological type, geometry of the impact (e.g. if tenuous gas is distributed around galaxies in flattened disks rather than in spherical halos), or disturbed morphologies or the presence of close companions (e.g. if tenuous gas is distributed around galaxies as a result of galaxy interactions). To determine these other factors, we have initiated a program to obtain and analyze HST Wide Field Planetary Camera 2 (WFPC2) images of galaxies identified in the survey.

Here we present initial results of this program, based on analysis of HST images of six fields obtained in Cycle 5 and four fields accessed from the HST archives. From these images, we measure properties of 87 galaxies, of which 33 are associated with corresponding Ly $\alpha$  absorption lines and 24 do not produce corresponding Ly $\alpha$  absorption lines to within sensitive upper limits. Considering only galaxy and absorber pairs that are likely to be physically associated and excluding galaxy and absorber pairs within  $3000 \text{ km s}^{-1}$  of the background QSOs leaves 26 galaxy and absorber pairs and seven galaxies that do not produce corresponding Ly $\alpha$  absorption lines to within sensitive upper limits. Redshifts of the galaxy and absorber pairs range from 0.0750 to 0.8912 with a median of 0.3718, and impact parameter separations of the galaxy and absorber pairs range from 12.4 to  $157.4 h^{-1}$  kpc with a median of  $62.4 h^{-1}$  kpc.

The resulting measurements are used to address a variety of issues: First, the measurements are used to examine how the incidence and extent of tenuous gas around galaxies depends on galaxy luminosity, size, and morphological type. Determining the fundamental scaling relationships between properties of the galaxies and properties of the absorbers is the first step toward understanding the nature and origin of the gas, analogous to establishing the Holmberg (1975) and Bosma (1981) relationships for the outer, tenuous parts of galaxies. Second, the measurements are used to examine the rough geometry of tenuous gas around galaxies. If galaxies are surrounded by spherical halos then they should exhibit absorption signatures that are independent of inclination and orientation, whereas if galaxies are surrounded by flattened disks then they should exhibit absorption preferentially at low inclination angles. Determining the rough distribution of tenuous gas around galaxies is crucial for distinguishing competing models of the origin of the gas. And finally, the measurements are used to examine the possibility that tenuous gas around galaxies results from galaxy interactions, as evidenced by disturbed morphologies and the presence of close companions.

The primary result of the analysis is that the amount of gas encountered along the line of sight depends on the galaxy impact parameter and  $B$ -band luminosity but does not depend strongly on the galaxy average surface brightness, disk-to-bulge ratio, or redshift. This result confirms and improves upon the anti-correlation between  $\text{Ly}\alpha$  absorption equivalent width and galaxy impact parameter found previously by Lanzetta et al. (1995) and argues that the gas is physically associated with the individual galaxies. Spherical halos cannot be distinguished from flattened disks on the basis of the current observations, and there is no evidence that galaxy interactions play an important role in distributing tenuous gas around galaxies in most cases. A dimensionless Hubble constant  $h = H_0/(100 \text{ km s}^{-1} \text{ Mpc}^{-1})$  and a deceleration parameter  $q_0 = 0.5$  are adopted throughout.

## 2. OBSERVATIONS

### 2.1. WFPC2 Imaging Observations

Imaging observations of the fields surrounding 0349–1438, 0405–1219, 0850+4400, 1001+2910, 1354+1933, and 1704+6048 were obtained with HST using WFPC2 with the F702W filter in Cycle 5. The observations were obtained in a series of three or four exposures of 600 or 800 s each. The journal of observations is given in Table 1, which lists the field, 1950 coordinates  $\alpha$  and  $\delta$  of the QSO, emission redshift  $z_{\text{em}}$  of the QSO, filter, exposure time, and date of observation.

Imaging observations of objects in the fields surrounding 0454–2203, 1545+2101, 1622+2352, and 2135–1446 were accessed from the HST archive. The observations were obtained with the HST using WFPC2 with the F606W or F702W filters. The observations were obtained in a series of between two and 24 exposures of between 100 and 1000 s each. The journal of archival observations is given in Table 2, which lists the field, 1950 coordinates  $\alpha$  and  $\delta$  of the QSO, emission redshift  $z_{\text{em}}$  of the QSO, filter, exposure time, and date of observation.

The individual exposures were reduced using standard pipeline techniques and were registered to a common origin, filtered for cosmic rays, and coadded using our own reduction programs. The final images are shown in Figure 1. The spatial resolution of the final images was measured to be FWHM  $\approx 0.1$  arcsec, and the  $5\sigma$  point source detection thresholds were measured to span the range  $m = 24.3$  through  $m = 28.8$ .

## 2.2. Other Observations

Detailed descriptions of the ground- and space-based imaging and spectroscopic observations have been and will be presented elsewhere (e.g. Lanzetta et al. 1995), but in summary the observations consist of (1) optical images and spectroscopy of objects in the fields of the QSOs, obtained with various telescopes and from the literature, and (2) ultraviolet spectroscopy of the QSOs, obtained with HST using the Faint Object Spectrograph (FOS) and accessed through the HST archive. These observations are summarized in Table 3, which for each field lists the number of galaxies (with spectroscopic redshifts) included into the analysis, the reference to the galaxy observations and analysis, the number of absorbers included into the analysis, and the reference to the absorber observations and analysis.

## 3. GALAXY IMAGE ANALYSIS

To determine structural parameters and angular inclinations and orientations of the galaxies, we apply a surface brightness  $\chi^2$  fitting program. The surface brightness  $I(R)$  as a function of galactocentric radius  $R$  is represented as the sum of an azimuthally symmetric exponential disk component and an azimuthally symmetric  $R^{1/4}$  bulge component

$$I(R) = I_{0D} \exp \left\{ -1.68 \left[ \frac{R}{R_D} - 1 \right] \right\} + I_{0B} \exp \left\{ -7.67 \left[ \left( \frac{R}{R_B} \right)^{1/4} - 1 \right] \right\}, \quad (1)$$

where  $R_D$  and  $R_B$  are the disk and bulge effective (or half-light) radii and  $I_{0D}$  and  $I_{0B}$  are the disk and bulge effective surface brightnesses (or surface brightnesses at the effective radii). (The exponential scale length of the disk component is  $R_D/1.68$ .) Galactocentric radius  $R$  is related to projected radius  $r$  and angle  $\theta$  to the projected line segment joining the galaxy to the QSO for the disk component by

$$R = r \left[ 1 + \sin^2(\theta + \alpha) \tan^2 i \right]^{1/2} \quad (2)$$

and for the bulge component by

$$R = r \left[ 1 + \sin^2(\theta + \alpha) \tan^2(\arccos b/a) \right]^{1/2}, \quad (3)$$

where  $\alpha$  is the orientation angle (measured north through east) between the apparent major axis of the galaxy and the projected line segment joining the galaxy to the QSO and  $i$  is the disk



inclination angle and  $b/a$  is the bulge axis ratio. The theoretical image is determined by convolving the surface brightness distribution described by equations (1), (2), and (3) with a model of the HST point spread function obtained with the Tiny Tim program (Krist 1995). The estimates of  $I_{0D}$ ,  $I_{0B}$ ,  $R_D$ ,  $R_B$ ,  $\alpha$ ,  $i$ , and  $b/a$  are determined by minimizing  $\chi^2$  as calculated from the theoretical image, the observed image, and the  $1\sigma$  error image, and the uncertainties are calculated from the the Hessian matrix at the minimum. The disk-to-bulge ratio  $D/B$  is the ratio of the integrated disk and bulge surface brightness profiles.

To determine the luminosities of the galaxies, we apply standard galaxy photometry techniques. The apparent magnitude  $m$  (in AB magnitude units at the wavelength centroid of the filter response function) is determined by directly integrating the theoretical surface brightness distribution within the Holmberg (1975) radius. The  $K$  correction is determined by integrating the product of the appropriate galaxy spectral energy distribution (selected by considering the galaxy spectral type) of Coleman, Wu, & Weedman (1980) and the appropriate filter response function and applying the appropriate bandpass correction. The rest-frame  $B$ -band absolute magnitude  $M_B - 5 \log h$  is determined from the apparent magnitude  $m$  and the  $K$  correction. The rest-frame  $B$ -band luminosity of an  $L_*$  galaxy (in AB magnitude units at  $B$ ) is taken to be  $M_{B*} = -19.5$  (Ellis et al. 1996).

To determine the rough morphological types of the galaxies, we consider the visual appearances, surface brightness distributions, and disk-to-bulge ratios  $D/B$ . Generally, galaxies with  $D/B < 3$  are classified as elliptical or S0 galaxies, galaxies with  $3 < D/B < 14$  are classified as early-type spiral galaxies, and galaxies with  $D/B > 14$  are classified as late-type spiral galaxies (Burstein 1979).

The results are summarized in the “Galaxies” portion of Table 4, which for each galaxy lists the field, Right Ascension and Declination offsets from the QSO  $\Delta\alpha$  and  $\Delta\delta$ , redshift  $z_{\text{gal}}$ , impact parameter  $\rho$ , disk and bulge effective radii  $R_D$  and  $R_B$ , disk-to-bulge ratio  $D/B$ , orientation angle  $\alpha$ , disk inclination angle  $i$ , bulge axis ratio  $b/a$ , apparent magnitude  $m$ , average surface brightness  $\langle\mu\rangle$  (within the Holmberg radius), and absolute  $B$ -band magnitude  $M_B - 5 \log h$ . Measurement uncertainties in  $R_D$  and  $R_B$  are typically 2%, measurement uncertainties in  $D/B$  are typically 35%, measurement uncertainties in  $\alpha$  and  $i$  are typically 2 deg, and measurement uncertainties in  $m$  and  $M_B - 5 \log h$  are typically 0.2.

#### 4. GALAXY AND ABSORBER PAIRS

Some galaxy and absorber pairs constitute *random* pairs, for which there is no physical relationship between the galaxy and the absorber. Random pairs dominate at velocity and impact parameter separations large in comparison to the scale on which galaxies cluster. Some galaxy and absorber pairs constitute *correlated* pairs, for which the galaxy is correlated with the galaxy that produces the absorber. Correlated pairs dominate at velocity and impact parameter separations

comparable to the scale on which galaxies cluster but large in comparison to the characteristic extent of tenuous gas around galaxies. And some galaxy and absorber pairs constitute *physical* pairs, for which the galaxy produces the absorber. Physical pairs dominate at velocity and impact parameter separations comparable to the characteristic extent of tenuous gas around galaxies. Because the goal of the analysis is to investigate tenuous gas around galaxies, it is necessary first to distinguish physical pairs from correlated and random pairs.

Physical and correlated pairs are easily statistically distinguished from random pairs by means of the galaxy–absorber cross-correlation function  $\xi_{\text{ga}}(v, \rho)$ . Specifically, a galaxy and absorber pair of velocity separation  $v$  and impact parameter separation  $\rho$  is likely to be a correlated or physical pair if the cross-correlation amplitude satisfies  $\xi_{\text{ga}}(v, \rho) > 1$  and is likely to be a random pair if the cross-correlation amplitude satisfies  $\xi_{\text{ga}}(v, \rho) < 1$ . Physical pairs are less easily distinguished from correlated pairs, because both can occur at relatively small velocity and impact parameter separations. To identify physical galaxy and absorber pairs we adopt the cross-correlation function  $\xi_{\text{ga}}(v, \rho)$  measured by Lanzetta, Webb, & Barcons (1997a,b) on the basis of 352 galaxies and 230 absorbers in 24 fields, from which 3126 galaxy and absorber pairs are formed. First, following Lanzetta et al. (1995) we accept Ly $\alpha$  absorption lines according to a  $3\sigma$  detection threshold criterion, which is appropriate because the measurements are performed at a small number of known galaxy redshifts. Next, we form galaxy and absorber pairs by requiring (1)  $\xi_{\text{ga}} > 1$  (which excludes likely random pairs) and (2)  $\rho < 200 h^{-1}$  kpc (which from results of Lanzetta, Webb, & Barcons 1997a,b excludes likely correlated pairs). Next, we exclude galaxy and absorber pairs within 3000 km s $^{-1}$  of the background QSOs (which are likely to be associated with the QSOs), and in cases where more than one galaxy is paired with one absorber we choose the galaxy at the smallest impact parameter. Finally, we measure  $3\sigma$  upper limits to Ly $\alpha$  absorption equivalent widths of galaxies that are not paired with corresponding absorbers, retaining only those measurements with  $3\sigma$  upper limits satisfying  $W < 0.35 \text{ \AA}$ . This procedure identifies 26 galaxy and absorber pairs and seven galaxies that do not produce corresponding Ly $\alpha$  absorption lines to within sensitive upper limits. Redshifts of the galaxy and absorber pairs range from 0.0750 to 0.8912 with a median of 0.3718, and impact parameter separations of the galaxy and absorber pairs range from 12.4 to 157.4  $h^{-1}$  kpc with a median of 62.4  $h^{-1}$  kpc.

The results are summarized in the “Absorbers” portion of Table 4, which for each galaxy lists the absorber redshift  $z_{\text{abs}}$  and Ly $\alpha$  absorption equivalent width  $W$ . Measurement uncertainties in  $W$  are typically 0.1  $\text{\AA}$ . In Table 4, galaxy entries without corresponding absorber entries represent cases for which the absorption measurement cannot be made, either because the galaxy occurs behind the QSO, the appropriate QSO spectrum is not available or lacks sensitivity, the spectral region containing the predicted Ly $\alpha$  line is blended with other absorption lines, or a corresponding Ly $\alpha$  absorption line was paired with a galaxy at a smaller impact parameter.

In adopting a quantitative criterion based on the galaxy–absorber cross-correlation function to distinguish physical pairs from correlated and random pairs, our analysis differs from the analyses of Le Brun, Bergeron, & Boissé (1996) and Bowen, Blades, & Pettini (1996), which failed to detect

the anti-correlation between Ly $\alpha$  absorption equivalent width and galaxy impact parameter. These analyses included galaxy and absorber pairs at impact parameter separations of up to 3800  $h^{-1}$  kpc, of which approximately 65% are at separations of more than 200  $h^{-1}$  kpc. At these large impact parameter separations, our evaluation using the galaxy–absorber cross-correlation function indicates vanishingly small probabilities of finding bona fide physical pairs. We believe that this difference in the analyses explains the differences in the results.

## 5. DESCRIPTIONS OF INDIVIDUAL FIELDS

Here we present brief descriptions of the individual fields, noting galaxies by their coordinate offsets in Right Ascension and Declination, respectively, from the QSO line of sight in units of 0.1 arcsec.

### 5.1. The Field toward 0349–1438

Galaxy –00094+00108 at  $z = 0.3567$  and  $\rho = 43.4 h^{-1}$  kpc is a late-type spiral galaxy of luminosity  $L_B = 0.62L_{B*}$ . This galaxy is associated with a corresponding Ly $\alpha$  absorption line at  $z = 0.3566$  with  $W = 0.94 \text{ \AA}$ .

Galaxies +00117–00241 at  $z = 0.3236$  and  $\rho = 77.0 h^{-1}$  kpc, –00292+00183 at  $z = 0.3244$  and  $\rho = 99.1 h^{-1}$  kpc, and +00126–00459 at  $z = 0.2617$  and  $\rho = 120.3 h^{-1}$  kpc are elliptical or S0 galaxies of luminosities between  $L_B = 0.30L_{B*}$  and  $L_B = 0.97L_{B*}$ . Galaxy –00571+00198 at  $z = 0.3273$  and  $\rho = 174.7 h^{-1}$  kpc is a late-type spiral galaxy of luminosity  $L_B = 0.73L_{B*}$ . These galaxies do not have sensitive Ly $\alpha$  absorption measurements available.

### 5.2. The Field toward 0405–1219

Galaxies +00106–00067 at  $z = 0.5714$  and  $\rho = 46.9 h^{-1}$  kpc, +00026–00150 at  $z = 0.5657$  and  $\rho = 56.8 h^{-1}$  kpc, +00104–00269 at  $z = 0.5779$  and  $\rho = 108.3 h^{-1}$  kpc, +00140–00354 at  $z = 0.5777$  and  $\rho = 143.0 h^{-1}$  kpc, and –00369+00354 at  $z = 0.5696$  and  $\rho = 191.1 h^{-1}$  kpc are elliptical or S0 galaxies of luminosities between  $L_B = 0.88L_{B*}$  and  $L_B = 1.98L_{B*}$ . These galaxies (which occur in the immediate vicinity of the QSO) do not produce corresponding Ly $\alpha$  absorption to within a sensitive upper limit.

Galaxy –00033–00127 at  $z = 0.5696$  and  $\rho = 49.0 h^{-1}$  kpc shows a disturbed morphology, to which normal disk and bulge profiles cannot be applied. This galaxy (which occurs in the immediate vicinity of the QSO) does not produce corresponding Ly $\alpha$  absorption to within a sensitive upper limit.

Galaxy +00010–00350 at  $z = 0.3520$  and  $\rho = 105.4 h^{-1}$  kpc is a late-type spiral galaxy of luminosity  $L_B = 0.28L_{B*}$ . This galaxy is associated with a corresponding Ly $\alpha$  absorption line at  $z = 0.3514$  with  $W = 0.70 \text{ \AA}$ .

Galaxy –00662–00309 at  $z = 0.1525$  and  $\rho = 126.3 h^{-1}$  kpc is a late-type spiral galaxy of luminosity  $L_B = 0.89L_{B*}$ . This galaxy is associated with a corresponding Ly $\alpha$  absorption line at  $z = 0.1532$  with  $W = 0.20 \text{ \AA}$ .

Galaxy –00372+00284 at  $z = 0.3617$  and  $\rho = 142.8 h^{-1}$  kpc is an elliptical or S0 galaxy of luminosity  $L_B = 3.21L_{B*}$ . This galaxy is associated with a corresponding Ly $\alpha$  absorption line at  $z = 0.3610$  with  $W = 0.77 \text{ \AA}$ .

Galaxy +00161–00451 at  $z = 0.6167$  and  $\rho = 183.9 h^{-1}$  kpc is a late-type spiral galaxy of luminosity  $L_B = 1.00L_{B*}$ . This galaxy occurs behind the QSO and so is excluded from all analysis.

Galaxy +00319–00479 at  $z = 0.2973$  and  $\rho = 157.4 h^{-1}$  kpc is an elliptical or S0 galaxy of luminosity  $L_B = 0.80L_{B*}$ . This galaxy is associated with a corresponding Ly $\alpha$  absorption line at  $z = 0.2980$  with  $W = 0.30 \text{ \AA}$ .

Galaxy –00656+00567 at  $z = 0.2800$  and  $\rho = 228.7 h^{-1}$  kpc shows signs of interaction and a disturbed morphology, to which normal disk and bulge profiles cannot be applied. This galaxy does not produce corresponding Ly $\alpha$  absorption to within a sensitive upper limit.

Galaxy +00192–00700 at  $z = 0.5170$  and  $\rho = 261.6 h^{-1}$  kpc is an late-type spiral galaxy of luminosity  $L_B = 0.70L_{B*}$ . This galaxy does not produce corresponding Ly $\alpha$  absorption to within a sensitive upper limit.

### 5.3. The Field toward 0454–2203

Galaxy +00106+00057 at  $z = 0.2784$  and  $\rho = 31.6 h^{-1}$  kpc is a late-type spiral galaxy of luminosity  $L_B = 0.22L_{B*}$ . This galaxy is associated with a corresponding Ly $\alpha$  absorption line at  $z = 0.2777$  with  $W = 0.81 \text{ \AA}$ .

Galaxy –00011–00180 at  $z = 0.4847$  and  $\rho = 63.3 h^{-1}$  kpc is a late-type spiral galaxy of luminosity  $L_B = 2.12L_{B*}$ , while galaxies –00182+00429 at  $z = 0.4836$  and  $\rho = 163.4 h^{-1}$  kpc, and +00378–00365 at  $z = 0.4837$  and  $\rho = 184.3 h^{-1}$  kpc are spiral galaxies of luminosity  $L_B \approx 1.9L_{B*}$ . These galaxies are associated with a corresponding Ly $\alpha$  absorption line at  $z = 0.4825$  with  $W = 1.54 \text{ \AA}$ . The small impact parameter of galaxy –00011–00180 suggests that it contributes most to the absorption line, although the modest impact parameters of galaxies –00182+00429 and +00378–00365 suggest that they also might contribute to the absorption line.

Galaxy +00042+00184 at  $z = 0.5325$  and  $\rho = 68.8 h^{-1}$  kpc is an elliptical or S0 galaxy of luminosity  $L_B = 0.47L_{B*}$ , and galaxy +00356–00410 at  $z = 0.5336$  and  $\rho = 198.1 h^{-1}$  kpc is a late-type spiral galaxy of luminosity  $L_B = 1.05L_{B*}$ . These galaxies (which occur in the immediate

vicinity of the QSO) do not produce corresponding Ly $\alpha$  absorption to within sensitive upper limits.

Galaxy +00003–00197 at  $z = 0.3818$  and  $\rho = 61.9 h^{-1}$  kpc is a late-type spiral galaxy of luminosity  $L_B = 0.64L_{B*}$ . This galaxy is associated with a corresponding Ly $\alpha$  absorption line at  $z = 0.3815$  with  $W = 0.46 \text{ \AA}$ . (A spiral arm of galaxy –00011–00180 points directly at galaxy +00003–00197, giving the impression that the two form an interacting pair. But in fact the two occur at cosmologically distinct redshifts.)

Galaxy +00145+00995 at  $z = 0.3382$  and  $\rho = 296.1 h^{-1}$  kpc is an early-type spiral galaxy of luminosity  $L_B = 0.76L_{B*}$ . This galaxy does not produce corresponding Ly $\alpha$  absorption to within a sensitive upper limit.

#### 5.4. The Field toward 0850+4400

Galaxy –00089+00020 at  $z = 0.1635$  and  $\rho = 16.6 h^{-1}$  kpc is an elliptical or S0 galaxy of luminosity  $L_B = 0.40L_{B*}$ . This galaxy is associated with a corresponding damped Ly $\alpha$  absorption line at  $z = 0.1630$  with  $W = 5.9 \text{ \AA}$ . This absorption system is the target of a recent investigation by Lanzetta et al. (1997c), which on the basis of a high-resolution spectrum obtained with HST using the Goddard High Resolution Spectrograph establishes a neutral hydrogen column density of  $\log N = 19.81 \pm 0.04 \text{ cm}^{-2}$ .

Galaxy +00100–00024 at  $z = 0.4402$  and  $\rho = 34.6 h^{-1}$  kpc is an S0 galaxy of luminosity  $L_B = 0.80L_{B*}$  with visible faint disk. This galaxy is associated with a corresponding Ly $\alpha$  absorption line at  $z = 0.4435$  with  $W = 0.51 \text{ \AA}$ .

Galaxy +00226+00124 at  $z = 0.5007$  and  $\rho = 91.7 h^{-1}$  kpc is a late-type spiral galaxy of luminosity  $L_B = 1.05L_{B*}$ . Galaxy +00455+00022 at  $z = 0.5196$  and  $\rho = 164.5 h^{-1}$  kpc is an elliptical or S0 galaxy of luminosity  $L_B = 2.22L_{B*}$ . These galaxies (which occur in the immediate vicinity of the QSO) do not produce corresponding Ly $\alpha$  absorption to within a sensitive upper limit.

Galaxy +00290+00305 at  $z = 0.2766$  and  $\rho = 110.2 h^{-1}$  kpc is a late-type spiral galaxy of luminosity  $L_B = 0.28L_{B*}$ . Galaxy –00005+00405 at  $z = 0.0915$  and  $\rho = 46.2 h^{-1}$  kpc is a late-type spiral galaxy of luminosity  $L_B = 0.07L_{B*}$ . Galaxy +00034+00350 at  $z = 0.0872$  and  $\rho = 38.5 h^{-1}$  kpc is an elliptical or S0 galaxy of luminosity  $L_B = 0.34L_{B*}$ . These galaxies do not have sensitive Ly $\alpha$  absorption measurements available.

#### 5.5. The Field toward 1001+2910

Galaxy –00034–00231 at  $z = 0.1380$  and  $\rho = 37.6 h^{-1}$  kpc is a late-type spiral galaxy of luminosity  $L_B = 0.03L_{B*}$ . This galaxy is associated with a corresponding Ly $\alpha$  absorption line at

$z = 0.1377$  with  $W = 0.67 \text{ \AA}$ .

Galaxy  $-00284+00066$  at  $z = 0.3308$  and  $\rho = 85.0 h^{-1} \text{ kpc}$  is an elliptical or S0 galaxy of luminosity  $L_B = 0.39L_{B^*}$ . This galaxy (which occurs in the immediate vicinity of the QSO) is associated with a corresponding Ly $\alpha$  absorption line at  $z = 0.3283$  with  $W = 0.18 \text{ \AA}$ .

### 5.6. The Field toward 1354+1933

Galaxy  $+00012+00075$  at  $z = 0.4592$  and  $\rho = 26.1 h^{-1} \text{ kpc}$  is a late-type spiral galaxy of luminosity  $L_B = 0.82L_{B^*}$ . This galaxy is associated with a corresponding Ly $\alpha$  absorption line at  $z = 0.4570$  with  $W = 1.41 \text{ \AA}$ .

Galaxy  $-00216-00122$  at  $z = 0.4406$  and  $\rho = 83.5 h^{-1} \text{ kpc}$  is an elliptical or S0 galaxy of luminosity  $L_B = 0.65L_{B^*}$ . This galaxy does not produce corresponding Ly $\alpha$  absorption to within a sensitive upper limit.

Galaxy  $-00160-00233$  at  $z = 0.4295$  and  $\rho = 94.1 h^{-1} \text{ kpc}$  is a late-type spiral galaxy of luminosity  $L_B = 0.38L_{B^*}$ . This galaxy is associated with a corresponding Ly $\alpha$  absorption line at  $z = 0.4306$  with  $W = 1.03 \text{ \AA}$ .

Galaxy  $-00134-00480$  at  $z = 0.5293$  and  $\rho = 181.3 h^{-1} \text{ kpc}$  is an elliptical or S0 galaxy of luminosity  $L_B = 0.91L_{B^*}$ . This galaxy does not produce corresponding Ly $\alpha$  absorption to within a sensitive upper limit.

Galaxy  $+00658+00501$  at  $z = 0.3509$  and  $\rho = 248.5 h^{-1} \text{ kpc}$  is an elliptical or S0 galaxy of luminosity  $L_B = 0.23L_{B^*}$ . This galaxy does not produce corresponding Ly $\alpha$  absorption to within a sensitive upper limit.

### 5.7. The Field toward 1545+2101

Galaxy  $-00027+00011$  at  $z = 0.2657$  and  $\rho = 7.2 h^{-1} \text{ kpc}$  is an elliptical or S0 galaxy of luminosity  $L_B = 0.67L_{B^*}$ , and galaxy  $+00166-00087$  at  $z = 0.2639$  and  $\rho = 47.6$  is an elliptical or S0 galaxy of luminosity  $L_B = 0.92L_{B^*}$ . These galaxies (which occur in the immediate vicinity of the QSO) are associated with a corresponding Ly $\alpha$  absorption line at  $z = 0.2641$  with  $W = 0.63$ . The small impact parameters of galaxies  $-00027-00011$  and  $+00166-00087$  suggest that both might contribute to the absorption line, although spectroscopic observations of four other galaxies toward 1545+2101 presented by Lanzetta, Webb, & Barcons (1996) indicate that these galaxies belong to a group or cluster of galaxies, several or all of which might contribute to the Ly $\alpha$  absorption line.

Galaxy  $-00263+00231$  at  $z = 0.1343$  and  $\rho = 55.1 h^{-1} \text{ kpc}$  is a late-type spiral galaxy of luminosity  $L_B = 0.22L_{B^*}$ . This galaxy does not produce corresponding Ly $\alpha$  absorption to within a sensitive upper limit. This is particularly striking because almost all other galaxies yet identified

at  $\rho < 100 h^{-1}$  kpc are associated with corresponding Ly $\alpha$  absorption lines, except for galaxies in the immediate vicinities of QSOs.

Galaxy +00273–00356 at  $z = 0.0949$  and  $\rho = 53.4 h^{-1}$  kpc is a late-type spiral galaxy of luminosity  $L_B = 0.03L_{B*}$ . This galaxy is associated with a corresponding Ly $\alpha$  absorption line at  $z = 0.0961$  with  $W = 0.18 \text{ \AA}$ .

### 5.8. The Field toward 1622+2352

The relationship between galaxies and absorption systems in this field was analyzed previously by Steidel et al. (1997), concentrating on metal-selected absorption systems. Our analysis differs from the analysis of Steidel et al. (1997) in two ways: (1) we applied the surface brightness analysis of § 3 to all galaxies with identified redshifts and (2) we accepted Ly $\alpha$  absorption lines according to a  $3\sigma$  detection threshold criterion and measured  $3\sigma$  upper limits to Ly $\alpha$  absorption equivalent widths of galaxies that are not paired with corresponding absorbers.

Galaxies –00015+00021 at  $z = 0.931$  and  $\rho = 10.9 h^{-1}$  kpc, +00073–00121 at  $z = 0.920$  and  $\rho = 59.5 h^{-1}$  kpc, +00088–00248 at  $z = 0.919$  and  $\rho = 111.0 h^{-1}$  kpc, and –00289+00057 at  $z = 0.923$  and  $\rho = 124.1 h^{-1}$  kpc are late-type spiral galaxies of luminosities in the range  $L_B = 0.31L_{B*}$  to  $3.04L_{B*}$ . Galaxies –00051+00111 at  $z = 0.920$  and  $\rho = 51.4 h^{-1}$  kpc, –00013+00113 at  $z = 0.921$  and  $\rho = 47.9 h^{-1}$  kpc, and –00264–00027 at  $z = 0.924$  and  $\rho = 111.8 h^{-1}$  kpc are elliptical or S0 galaxies of luminosities  $L_B = 0.81L_{B*}$  and  $3.38L_{B*}$ , respectively. These galaxies (which occur in the immediate vicinity of the QSO) do not produce corresponding Ly $\alpha$  absorption to within a sensitive upper limit.

Galaxy +00030–00000 at  $z = 0.892$  and  $\rho = 12.4 h^{-1}$  kpc is a highly inclined late-type spiral galaxy of luminosity  $L_B = 0.65L_{B*}$ , and galaxy –00076–00434 at  $z = 0.892$  and  $\rho = 184.6 h^{-1}$  kpc is a late-type spiral galaxy of luminosity  $L_B = 0.44L_{B*}$ . These two galaxies are associated with a corresponding Ly $\alpha$  absorption line at  $z = 0.8909$  with  $W = 2.71 \text{ \AA}$ . The small impact parameter of galaxy +00030–00000 suggests that it contributes most to the absorption line.

Galaxy –00042–00038 at  $z = 0.4720$  and  $\rho = 19.5 h^{-1}$  kpc is a late-type spiral galaxy of luminosity  $L_B = 0.22L_{B*}$ . This galaxy is associated with a corresponding Ly $\alpha$  absorption line at  $z = 0.4716$  with  $W = 0.91 \text{ \AA}$ . This absorption system is noted as an upper-limit in the sample of Steidel et al. (1996).

Galaxy –00055+00075 at  $z = 0.6352$  and  $\rho = 36.3 h^{-1}$  kpc is a late-type spiral galaxy of luminosity  $L_B = 0.11L_{B*}$ . This galaxy is associated with a corresponding Ly $\alpha$  absorption line at  $z = 0.6359$  with  $W = 0.47 \text{ \AA}$ .

Galaxy –00089+00032 at  $z = 0.798$  and  $\rho = 39.0 h^{-1}$  kpc is a late-type spiral galaxy of luminosity  $L_B = 1.05L_{B*}$ . This galaxy is associated with a corresponding Ly $\alpha$  absorption line at  $z = 0.7964$  with  $W = 1.37 \text{ \AA}$ .

Galaxy  $-00033+00091$  at  $z = 0.5650$  and  $\rho = 36.0 h^{-1}$  kpc is an elliptical or S0 galaxy of luminosity  $L_B = 0.10L_{B*}$ . This galaxy does not produce corresponding Ly $\alpha$  absorption to within a sensitive upper limit.

Galaxy  $+00016+00142$  at  $z = 0.656$  and  $\rho = 55.9 h^{-1}$  kpc is a late-type spiral galaxy of luminosity  $L_B = 0.43L_{B*}$ . This galaxy is associated with a corresponding Ly $\alpha$  absorption line at  $z = 0.6564$  with  $W = 7.75 \text{ \AA}$ . Although the Ly $\alpha$  absorption equivalent width associated with this galaxy appears to be particularly large given the relatively large impact parameter of the galaxy, Steidel et al. (1996) were unable to identify another galaxy at a smaller impact parameter despite an intensive search.

Galaxy  $-00123+00099$  at  $z = 0.7016$  and  $\rho = 73.4 h^{-1}$  kpc is a late-type spiral galaxy of luminosity  $L_B = 1.11L_{B*}$ . This galaxy is associated with a corresponding Ly $\alpha$  absorption line at  $z = 0.7020$  with  $W = 0.48 \text{ \AA}$ .

Galaxy  $+00079-00170$  at  $z = 0.828$  and  $\rho = 77.7 h^{-1}$  kpc is an elliptical or S0 galaxy of luminosity  $L_B = 0.35L_{B*}$ . This galaxy is associated with a corresponding Ly $\alpha$  absorption line at  $z = 0.8273$  with  $W = 1.06 \text{ \AA}$ .

Galaxy  $-00079+00307$  at  $z = 0.7090$  and  $\rho = 126.7 h^{-1}$  kpc is a late-type spiral galaxy of luminosity  $L_B = 0.16L_{B*}$ . This galaxy is associated with a corresponding Ly $\alpha$  absorption line at  $z = 0.7090$  with  $W = 0.20 \text{ \AA}$ . This absorption system is not contained in the sample of Steidel et al. (1996).

Galaxies  $-00111-00043$  at  $z = 1.037$  and  $\rho = 51.0 h^{-1}$  kpc,  $+00182+00002$  at  $z = 1.010$  and  $\rho = 77.7 h^{-1}$  kpc,  $+00150+00196$  at  $z = 1.018$  and  $\rho = 105.2 h^{-1}$  kpc, and  $-00343+00032$  at  $z = 1.011$  and  $\rho = 146.9 h^{-1}$  kpc show disturbed morphologies. These galaxies occur behind the QSO and so are excluded from all analysis.

Galaxies  $-00067+00097$  at  $z = 0.318$  and  $\rho = 33.6 h^{-1}$  kpc,  $-00213-00062$  at  $z = 0.368$  and  $\rho = 68.4 h^{-1}$  kpc,  $-00241+00053$  at  $z = 0.368$  and  $\rho = 75.9 h^{-1}$  kpc,  $+00255+00176$  at  $z = 0.261$  and  $\rho = 78.1 h^{-1}$  kpc,  $+00127-00312$  at  $z = 0.280$  and  $\rho = 88.9 h^{-1}$  kpc,  $-00454+00077$  at  $z = 0.668$  and  $\rho = 181.1 h^{-1}$  kpc, and  $-00468+00077$  at  $z = 0.638$  and  $\rho = 183.9 h^{-1}$  kpc together show morphologies in the range elliptical or S0 galaxies to late-type spiral galaxies of luminosities in the range  $L_B = 0.03L_{B*}$  to  $1.35L_{B*}$ . These galaxies do not have sensitive Ly $\alpha$  absorption measurements available.

### 5.9. The Field toward 1704+6048

Galaxy  $+00081-00271$  at  $z = 0.3615$  and  $\rho = 86.4 h^{-1}$  kpc is a late-type spiral galaxy of luminosity  $L_B = 0.68L_{B*}$ . This galaxy (which occurs at the immediate vicinity of the QSO) is associated with a corresponding Ly $\alpha$  absorption line at  $z = 0.3621$  with  $W = 0.67 \text{ \AA}$ .



Galaxy +00268–00352 at  $z = 0.3731$  and  $\rho = 136.9 h^{-1}$  kpc is an elliptical or S0 galaxy of luminosity  $L_B = 1.32L_{B*}$ . This galaxy (which occurs at the immediate vicinity of the QSO) is associated with a corresponding Ly $\alpha$  absorption line at  $z = 0.3716$  with  $W = 0.36 \text{ \AA}$ .

Galaxy –00510+00183 at  $z = 0.0921$  and  $\rho = 62.2 h^{-1}$  kpc is an early-type spiral galaxy of luminosity  $L_B = 0.19L_{B*}$ . This galaxy is associated with a corresponding Ly $\alpha$  absorption line at  $z = 0.0920$  with  $W = 0.89 \text{ \AA}$ . This galaxy was studied previously by Barcons, Lanzetta, & Webb (1995).

Galaxy –00700+00133 at  $z = 0.2260$  and  $\rho = 163.6 h^{-1}$  kpc is a late-type spiral galaxy of luminosity  $L_B = 0.14L_{B*}$ . This galaxy does not produce corresponding Ly $\alpha$  absorption to within a sensitive upper limit.

Galaxy +00729+00059 at  $z = 0.1877$  and  $\rho = 147.4 h^{-1}$  kpc is an elliptical or S0 galaxy of luminosity  $L_B = 0.78L_{B*}$ . This galaxy is associated with a corresponding Ly $\alpha$  absorption line at  $z = 0.1880$  with  $W = 0.43 \text{ \AA}$ .

Galaxy +00544+00102 at  $z = 0.4033$  and  $\rho = 178.7 h^{-1}$  kpc is a late-type spiral galaxy of luminosity  $L_B = 0.35L_{B*}$ . This galaxy occurs behind the QSO and so is excluded from all analysis.

Galaxies –00313–00094 at  $z = 0.3380$  and  $\rho = 96.2 h^{-1}$  kpc and –00142–00304 at  $z = 0.0713$  and  $\rho = 30.8 h^{-1}$  kpc are late-type spiral galaxies of luminosities  $L_B = 0.25L_{B*}$  and  $L_B = 0.007L_{B*}$ , respectively. These galaxies do not have sensitive Ly $\alpha$  absorption measurements available.

### 5.10. The Field toward 2135–1446

Galaxies +00047–00026 at  $z = 0.1996$  and  $\rho = 11.3 h^{-1}$  kpc, –00073+00157 at  $z = 0.2000$  and  $\rho = 36.6 h^{-1}$  kpc, and +00186–00335 at  $z = 0.1991$  and  $\rho = 80.8 h^{-1}$  kpc, are elliptical or S0 galaxies of luminosities in the range  $L_B = 0.39L_{B*}$  to  $0.61L_{B*}$ . Galaxy +00131–00217 at  $z = 0.1986$  and  $\rho = 53.3 h^{-1}$  kpc and +00284–00313 at  $z = 0.2011$  and  $\rho = 89.6 h^{-1}$  kpc are late-type spiral galaxies of luminosities  $L_B = 0.25L_{B*}$  and  $L_B = 1.89L_{B*}$ , respectively. These galaxies (which occur in the immediate vicinity of the QSO) are associated with a corresponding Ly $\alpha$  absorption line at  $z = 0.2005$  with  $W = 1.80 \text{ \AA}$ . The small impact parameters of galaxies +00047–00026, –00073+00157, +00131–00217, +00186–00335, and +00284–00313 suggest that all might contribute to the absorption line. Another galaxy just 1.9 arcsec from the QSO is visible in the image of +00047–00026. If this galaxy is at the redshift  $z \approx 0.20$  of the other galaxies, it occurs at an impact parameter of only  $\rho = 4.0 h^{-1}$  kpc.

Galaxy –00008+00493 at  $z = 0.0752$  and  $\rho = 47.8 h^{-1}$  kpc is a late-type spiral galaxy of luminosity  $L_B = 0.27L_{B*}$ . This galaxy is associated with a corresponding Ly $\alpha$  absorption line at  $z = 0.0750$  with  $W = 0.33 \text{ \AA}$ . This galaxy was studied previously by Barcons, Lanzetta, & Webb (1995).

Galaxy +00508–00217 at  $z = 0.1857$  and  $\rho = 111.0 h^{-1}$  kpc is a late-type spiral galaxy of luminosity  $L_B = 0.41L_{B*}$ . This galaxy is associated with a corresponding Ly $\alpha$  absorption line at  $z = 0.1848$  with  $W = 1.29 \text{ \AA}$ .

## 6. ANALYSIS

### 6.1. Method of Analysis

The goals of the analysis are (1) to demonstrate the existence of a fiducial relationship between some measure of the strength of neutral hydrogen absorption (e.g. Ly $\alpha$  absorption equivalent width  $W$  or neutral hydrogen column density  $N$ ) and galaxy impact parameter and (2) to assess whether accounting for measurements of other galaxy properties (besides galaxy impact parameter) can improve upon the fiducial relationship. Conceptually, we divide the the available measurements into a “dependent measurement”  $y$  of the strength of neutral hydrogen absorption and various “independent measurements”  $x_1, x_2, \dots$  of galaxy properties. For the dependent measurement we consider variously  $\log W$ ,  $\log(W \cos i)$ ,  $\log N$ , and  $\log(N \cos i)$ . (The  $\cos i$  factor is included as a path-length correction in models of inclined galaxy disks.) For the independent measurements we consider variously combinations of  $\log \rho$ ,  $\log L_B$ ,  $\log r_e$ ,  $\langle \mu \rangle$ ,  $\log D/B$ , and  $\log(1+z)$ . The goals of the analysis are equivalent to searching for a “fundamental surface” in a multi-dimensional space spanned by the dependent measurements and various combinations of the independent measurements.

To determine the functional form of the relationship between the dependent and the independent measurements, we adopt a parameterized functional dependence

$$y = y(x_1, x_2, \dots) \quad (4)$$

and apply a maximum-likelihood analysis to estimate the parameters and their uncertainties. In practice, we consider the independent measurements one or two at a time and adopt a linear or bi-linear relationship between the dependent and the independent measurements

$$y = a_1 x_1 + \text{constant} \quad (5)$$

or

$$y = a_1 x_1 + a_2 x_2 + \text{constant}, \quad (6)$$

where  $x_1$  is always  $\log \rho$  and  $x_2$  is some other galaxy property. (Except for the independent measurements  $\langle \mu \rangle$ , the dependent and the independent measurements are always logarithms of actual observed quantities, so in these cases equations 5 and 6 are equivalent to power-law relationships between the actual observed quantities.) Because the observations include both measurements and upper limits, the likelihood function is taken to be

$$\mathcal{L} = \left( \prod_{i=1}^n \exp \left\{ -\frac{1}{2} \left[ \frac{y_i - y(x_{1i}, x_{2i})}{\sigma_i} \right]^2 \right\} \right) \left( \prod_{i=1}^m \int_{y_i}^{-\infty} dy' \exp \left\{ -\frac{1}{2} \left[ \frac{y' - y(x_{1i}, x_{2i})}{\sigma_i} \right]^2 \right\} \right), \quad (7)$$

where  $\sigma_i$  is the uncertainty of the dependent measurement and where the first product extends over the  $n$  measurements and the second product extends over the  $m$  upper limits. (This definition of the likelihood function is appropriate if the residuals about the mean relationship are normally distributed.) Because  $\sigma_i$  may include significant “cosmic” scatter (which presumably arises due to intrinsic variations between individual galaxies) as well as measurement error,  $\sigma_i$  is taken to be the quadratic sum of the cosmic scatter  $\sigma_c$  and the measurement error  $\sigma_{m_i}$

$$\sigma_i^2 = \sigma_c^2 + \sigma_{m_i}^2, \quad (8)$$

where the cosmic scatter is defined by

$$\sigma_c^2 = \text{med} \left( \left\{ y_i - y(x_{1_i}, x_{2_i}) - \frac{1}{n} \sum_{j=1}^n [y_j - y(x_{1_j}, x_{2_j})] \right\}^2 - \sigma_{m_i}^2 \right). \quad (9)$$

Because  $\sigma_c$  depends on the maximum-likelihood solution  $y(x_{1_i}, x_{2_i})$ , the maximum-likelihood solution is obtained iteratively with respect to equations (7) and (9).

To assess the statistical significance of the relationship between the dependent and the independent measurements, we apply two statistical tests of the null hypothesis that the dependent and the independent measurements are unrelated. First, we apply a “confidence interval test” by using the likelihood function to evaluate the  $1\sigma$  confidence interval on the parameters. Under the null hypothesis,  $a_1 = a_2 = 0$  to within measurement error, so a significant measurement of  $a_1 \neq 0$  or  $a_2 \neq 0$  invalidates the null hypothesis. Second, we apply an “anti-correlation test” by using the generalized (to treat upper limits) Kendall, Kendall, Spearman, and Pearson correlation tests to evaluate the correlation between the dependent measurements and a “reduced” combination of the independent measurements  $x_1 + (a_2/a_1)x_2$ . (In applying the Kendall, Spearman, and Pearson correlation tests, which are not designed to treat upper limits,  $3\sigma$  upper limits are included as detections.) Under the null hypothesis the dependent and independent measurements are uncorrelated, so a significant measurement of a correlation invalidates the null hypothesis. Results of the statistical tests are presented in Table 5, which lists the measurements; the statistical significances  $a/\delta a$  of the fitting coefficients; the correlation coefficients  $r_{gk}$ ,  $r_k$ ,  $r_s$ , and  $r_p$  and statistical significances  $r_{gk}/\sigma_{gk}$ ,  $r_k/\sigma_k$ ,  $r_s/\sigma_s$ , and  $r_p/\sigma_p$  of the generalized Kendall, Kendall, Spearman, and Pearson correlation tests, respectively; and the cosmic scatter  $\sigma_c$ .

## 6.2. Galaxy Impact Parameter

In this section, we assess the possibility that the amount of gas intercepted along the line of sight depends on galaxy impact parameter  $\rho$  by adopting a power-law relationship between  $W$  and  $\rho$

$$\log W = -\alpha \log \rho + \text{constant} \quad (10)$$

and applying the analysis of § 6.1 to the measurements of § 3. The maximum-likelihood analysis yields

$$\alpha = 0.93 \pm 0.13, \quad (11)$$

and the results of the statistical tests are given in row 1 of Table 5. The relationship between  $W$  and  $\rho$  is shown in Figure 2.

The results summarized in Table 5 indicate that  $W$  is anti-correlated with  $\rho$ . Specifically, the confidence interval test indicates that  $\alpha$  differs from zero at the  $7.2\sigma$  level of significance, and the anti-correlation test indicates that  $W$  is anti-correlated with  $\rho$  at a level of significance ranging from  $3.36\sigma$  through  $4.45\sigma$ . We conclude that the amount of gas intercepted along the line of sight depends on galaxy impact parameter, which argues that the gas is physically associated with the individual galaxies.

### 6.3. Galaxy $B$ -Band Luminosity

In this section, we assess the possibility that the the amount of gas intercepted along the line of sight depends on galaxy  $B$ -band luminosity  $L_B$  by adopting a power-law relationship between  $W$  and  $\rho$  and  $L_B$

$$\log W = -\alpha \log \rho + \beta \log L_B + \text{constant} \quad (12)$$

and applying the analysis of § 6.1 to the measurements of § 3. The maximum-likelihood analysis yields

$$\alpha = 1.02 \pm 0.12 \quad (13)$$

and

$$\beta = 0.37 \pm 0.10, \quad (14)$$

and the results of the statistical tests are given in row 2 of Table 5. The relationship between  $W$  and  $\rho$  and  $L_B$  is shown in Figure 3.

The results summarized in Table 5 indicate that the relationship between  $W$  and  $\rho$  accounting for  $L_B$  is superior to the fiducial relationship between  $W$  and  $\rho$ . Specifically, the confidence interval test indicates that  $\beta$  differs from zero at the  $3.7\sigma$  level of significance, and the anti-correlation test indicates that the anti-correlation between  $W$  and  $\rho$  accounting for  $L_B$  is stronger and more significant than the anti-correlation between  $W$  and  $\rho$ , at a level of significance ranging from  $4.26\sigma$  to  $5.79\sigma$ . We conclude that the amount of gas intercepted along the line of sight depends on galaxy  $B$ -band luminosity. This result applies over the  $B$ -band luminosity interval  $0.007L_{B*} \lesssim L_B \lesssim 3.4L_{B*}$  spanned by the observations.

#### 6.4. Galaxy Effective Radius

In this section, we assess the possibility that the amount of gas intercepted along the line of sight depends on galaxy effective radius  $r_e$  by adopting a power-law relationship between  $W$  and  $\rho$  and  $r_e$

$$\log W = -\alpha \log \rho + \eta \log r_e + \text{constant} \quad (15)$$

and applying the analysis of § 6.1 to the measurements of § 3. The results of the statistical tests are given in row 3 of Table 5.

The results summarized in Table 5 indicate that the relationship between  $W$  and  $\rho$  accounting for  $r_e$  is superior to the fiducial relationship between  $W$  and  $\rho$  but marginally inferior to the relationship between  $W$  and  $\rho$  accounting for  $L_B$ . Specifically, the confidence interval test indicates that  $\eta$  differs from zero at the  $3.7\sigma$  level of significance, and the anti-correlation test indicates that the anti-correlation between  $W$  and  $\rho$  accounting for  $r_e$  is stronger and more significant than the anti-correlation between  $W$  and  $\rho$  although neither as strong nor as significant than the anti-correlation between  $W$  and  $\rho$  accounting for  $L_B$ . The similarity between results accounting for  $L_B$  and results accounting for  $r_e$  is plausible given the Holmberg (1975) correlation between galaxy luminosity and size. We conclude that the amount of gas intercepted along the line of sight depends on galaxy effective radius, but only indirectly through the correlation between galaxy effective radius and galaxy  $B$ -band luminosity. This result applies over the effective radius interval  $0.2 \lesssim r_e \lesssim 7.1 h^{-1}$  kpc spanned by the observations.

#### 6.5. Galaxy Average Surface Brightness

In this section, we assess the possibility that the amount of gas intercepted along the line of sight depends on galaxy average surface brightness  $\langle\mu\rangle$  by adopting a power-law relationship between  $W$  and  $\rho$  and  $\langle\mu\rangle$

$$\log W = -\alpha \log \rho + \lambda \langle\mu\rangle + \text{constant}. \quad (16)$$

and again applying the analysis of § 6.1 to the measurements of § 3. The results of the statistical tests are given in row 4 of Table 5.

The results summarized in Table 5 indicate that the relationship between  $W$  and  $\rho$  accounting for  $\langle\mu\rangle$  is statistically identical to the fiducial relationship between  $W$  and  $\rho$ . We conclude that the amount of gas intercepted along the line of sight does not depend strongly on galaxy average surface brightness. This result applies over the average surface brightness interval  $21.3 \lesssim \langle\mu\rangle \lesssim 26.4$  mag arcsec $^{-2}$  spanned by the observations.

### 6.6. Galaxy Disk-to-Bulge Ratio

In this section, we assess the possibility that the amount of gas intercepted along the line of sight depends on galaxy disk-to-bulge ratio  $D/B$  by adopting a power-law relationship between  $W$  and  $\rho$  and  $D/B$

$$\log W = -\alpha \log \rho + \delta \log D/B + \text{constant}. \quad (17)$$

and again applying the analysis of § 6.2 to the measurements of § 3. The results of the statistical tests are given in row 5 of Table 5.

The results summarized in Table 5 indicate that the relationship between  $W$  and  $\rho$  accounting for  $D/B$  is marginally superior to the fiducial relationship between  $W$  and  $\rho$  but marginally inferior to the relationship between  $W$  and  $\rho$  accounting for  $L_B$ . We conclude that the amount of gas intercepted along the line of sight does not depend strongly on galaxy disk-to-bulge ratio. This result applies over the disk-to-bulge ratio interval of bulge-dominated to disk-dominated galaxies spanned by the observations.

### 6.7. Redshift

In this section, we assess the possibility that the amount of gas intercepted along the line of sight depends on redshift  $z$  by adopting a power-law relationship between  $W$  and  $\rho$  and  $1+z$

$$\log W = -\alpha \log \rho + \gamma \log(1+z) + \text{constant}. \quad (18)$$

and again applying the analysis of § 6.2 to the measurements of § 3. The results of the statistical tests are given in row 6 of Table 5.

The results summarized in Table 5 indicate that the relationship between  $W$  and  $\rho$  accounting for  $z$  is statistically identical to the fiducial relationship between  $W$  and  $\rho$ . We conclude that the amount of gas intercepted along the line of sight does not depend strongly on redshift. This result applies over the redshift interval  $0.1 \lesssim z \lesssim 0.8$  spanned by the observations.

### 6.8. Shape of Tenuous Gas around Galaxies

In this section, we assess the possibility that tenuous gas is distributed around galaxies in flattened disks rather than in spherical halos by repeating the analyses of §§ 6.2 through 6.7, substituting  $W$  or  $W \cos i$  for  $W$  and galaxy galactocentric distance  $R$  for galaxy impact parameter  $\rho$ . If tenuous gas is distributed around galaxies in flattened disks, then the strength of neutral hydrogen absorption should vary as a function of  $R$  rather than  $\rho$ . (Galactocentric radius  $R$  is related to impact parameter  $\rho$  through the inclination and orientation angles  $i$  and  $\alpha$ .) In the optically thick limit, the Ly $\alpha$  absorption equivalent width should be independent of path length

through the disk, hence the Ly $\alpha$  absorption equivalent width corrected to face-on inclination is  $W$ . In the optically thin limit, the Ly $\alpha$  absorption equivalent width should vary as the path length through the disk, or in other words as  $1/\cos i$ , hence the Ly $\alpha$  absorption equivalent width corrected to face-on inclination is  $W \cos i$ . The results of the statistical tests are given in rows 7 through 13 of Table 5, and the relationship between  $W \cos i$  and  $R$  is shown in Figure 4.

The results summarized in Table 5 indicate that the relationships between  $W$  and  $R$  or  $W \cos i$  and  $R$  are statistically identical to the fiducial relationship between  $W$  and  $\rho$ . We conclude that spherical halos cannot be distinguished from flattened disks on the basis of the current observations.

### 6.9. Column Density Distribution of Tenuous Gas around Galaxies

In this section, we assess the possibility that tenuous gas around galaxies is better described by a relationship in neutral hydrogen column density  $N$  than by a relationship in Ly $\alpha$  absorption equivalent width by repeating the analyses of §§ 6.2 through 6.8 substituting  $N$  or  $N \cos i$  for  $W$  or  $W \cos i$ . Following Lanzetta et al. (1995), we estimate neutral hydrogen column densities from Ly $\alpha$  absorption equivalent widths by applying a curve-of-growth analysis, assuming that the Doppler parameters are contained in the range  $20 < b < 40 \text{ km s}^{-1}$ . The results of the statistical tests are given in rows 14 through 26 of Table 5.

The results summarized in Table 5 indicate that the relationship between  $N$  and  $\rho$  or  $N$  and  $R$  are marginally superior to the relationships between  $W$  and  $\rho$  or  $W$  and  $R$ . We conclude that tenuous gas around galaxies is marginally better described by a relationship in neutral hydrogen column density than by a relationship in Ly $\alpha$  absorption equivalent width.

As a summary of the results of the preceding sections, we derive the column density distribution of tenuous gas around galaxies, incorporating significant scaling relationships and rejecting insignificant scaling relationships. The results of §§ 6.2 through 6.8 indicate that neutral hydrogen column density depends on  $\rho$  and  $L_B$  but does not depend strongly on  $\langle \mu \rangle$ ,  $D/B$ , or  $z$  and that spherical halos cannot be distinguished from flattened disks on the basis of the current observations. Accordingly we adopt a power-law relationship between  $N$  and  $\rho$  and  $L_B$

$$\log \left( \frac{N}{10^{20} \text{ cm}^{-2}} \right) = -\alpha \log \left( \frac{\rho}{10 \text{ kpc}} \right) + \beta \log \left( \frac{L_B}{L_{B*}} \right) + \text{constant} \quad (19)$$

and apply the analysis of § 6.1 to the measurements of § 3. The maximum-likelihood analysis yields

$$\alpha = 5.33 \pm 0.50, \quad (20)$$

$$\beta = 2.19 \pm 0.55, \quad (21)$$

and

$$\text{constant} = 1.09 \pm 0.90. \quad (22)$$

The cosmic scatter about this relationship is

$$\sigma_c = 0.815, \quad (23)$$

which corresponds to a factor of  $\approx 6.5$  in neutral hydrogen column density. Substituting values from equations (20), (21), and (22) into equation (19), our current best estimate of the column density distribution of tenuous gas around galaxies is

$$\log \left( \frac{N}{10^{20} \text{ cm}^{-2}} \right) = -5.33 \log \left( \frac{\rho}{10 \text{ kpc}} \right) - 2.19 \log \left( \frac{L_B}{L_{B_*}} \right) + 1.09. \quad (24)$$

The relationship between  $N$  and  $\rho$  and  $L_B$  is shown in Figure 5.

### 6.10. Galaxy Morphology

The analyses of §§ 6.5 and 6.6 indicate that the amount of gas intercepted along the line of sight does not depend strongly on galaxy surface brightness or galaxy disk-to-bulge ratio. Because both galaxy surface brightness and galaxy disk-to-bulge ratio are correlated with morphological type, this implies that the amount of gas intercepted along the line of sight does not depend strongly on morphological type. Furthermore, the morphological types of galaxies that produce corresponding Ly $\alpha$  absorption lines are directly observed to range from elliptical or S0 galaxies (e.g. galaxy –00284+00066 toward 1001+2910) through early-type spiral galaxies (e.g. galaxy +00508–00217 toward 2135–1446) through late-type spiral galaxies (e.g. galaxy +00273–00356 toward 1545+2101). We conclude that galaxies that produce Ly $\alpha$  absorption systems span a wide range of morphological types.

### 6.11. Galaxy Interactions

Of the galaxies shown in Figure 1, only galaxies –00033–00127 and –00656+00567 toward 0405–1219 appear to exhibit obvious signs of disturbed morphologies. Galaxy –00033–00127 occurs in the immediate vicinity of the QSO and does not produce a corresponding Ly $\alpha$  absorption line to within a sensitive upper limit. Galaxy –00656+00567 appears to be in a “post-merger” stage with a visible asymmetric ring surrounding the nucleus. This galaxy does not produce a corresponding Ly $\alpha$  absorption lines to within a sensitive upper limit, although it occurs at a relatively large impact parameter ( $\rho = 228.7 h^{-1} \text{ kpc}$ ). We conclude that there is no evidence that tenuous gas is distributed around galaxies as a result of galaxy interactions in most cases, although it is of course possible that tenuous gas is distributed around galaxies as a result of galaxy interactions in some cases.



## 7. DISCUSSION

The primary result of the analysis is that the amount of gas encountered along the line of sight depends on the galaxy impact parameter  $\rho$  and  $B$ -band luminosity  $L_B$  but does not depend strongly on the galaxy average surface brightness  $\langle\mu\rangle$ , disk-to-bulge ratio  $D/B$ , or redshift  $z$ . Apparently extended gaseous envelopes are a common and generic feature of galaxies of a wide range of luminosity and morphological type, and Ly $\alpha$  absorption systems trace a significant and representative portion of the galaxy population. The most important implication of this result is that it provides for the first time a means of quantitatively relating statistical properties of Ly $\alpha$  absorption systems to statistical properties of faint galaxies.

First, we determine the relationship between galaxy gaseous radius  $r$  and galaxy  $B$ -band luminosity  $L_B$ , which is analogous to the Holmberg (1975) relationship between galaxy stellar radius and galaxy  $B$ -band luminosity. Adopting the power-law relationship between  $W$  and  $\rho$  and  $L_B$  of equation (12), the relationship between  $r$  and  $L_B$  at a fixed Ly $\alpha$  absorption equivalent width threshold is

$$\frac{r}{r_*} = \left( \frac{L_B}{L_{B*}} \right)^t, \quad (25)$$

where  $r_*$  is the gaseous radius of an  $L_*$  galaxy and where  $t = \beta/\alpha$ . Adopting  $\alpha$  and  $\beta$  from equations (13) and (14) yields

$$t = 0.37 \pm 0.11, \quad (26)$$

and adopting the maximum-likelihood analysis value of the constant of equation (12) yields

$$r_* = 174^{+38}_{-25} h^{-1} \text{ kpc} \quad (27)$$

for a Ly $\alpha$  absorption equivalent width threshold  $W = 0.3 \text{ \AA}$ . This result applies over the  $B$ -band luminosity interval  $0.007 \lesssim L_B \lesssim 3.4L_{B*}$  spanned by the observations. The value of  $r_*$  that we derive here agrees completely with previous results of Lanzetta et al. (1995).

Next, we apply the relationship between galaxy gaseous radius and galaxy  $B$ -band luminosity to predict the incidence of Ly $\alpha$  absorption systems produced by galaxies drawn from a known galaxy luminosity function. Integrating over galaxies of  $B$ -band luminosity  $L_B > L_{B_{\min}}$ , the predicted number density per line of sight  $n(z)$  of Ly $\alpha$  absorption systems is

$$n(z) = \frac{c}{H_0} (1+z)(1+2q_0z)^{-1/2} \int_{L_{B_{\min}}}^{\infty} dL_B \Phi(L_B, z) \pi r^2(L_B) \kappa \epsilon, \quad (28)$$

where  $c$  is the speed of light,  $\Phi(L_B, z)$  is the galaxy luminosity function,  $\kappa$  is the halo covering factor (averaged over all inclination angles), and  $\epsilon$  is the fraction of galaxies that produce corresponding Ly $\alpha$  absorption systems. Applying equation (25) and adopting a Schechter (1976) galaxy luminosity function  $\Phi(L_B) = \Phi_*(L_B/L_{B*})^{-s} \exp(-L_B/L_{B*})$ , the predicted number density per line of sight of Ly $\alpha$  absorption systems is

$$n(z) = \frac{c}{H_0} (1+z)(1+2q_0z)^{-1/2} \pi r_*^2 \kappa \epsilon \Phi_* \Gamma(1+2t-s, L_{B_{\min}}/L_{B*}), \quad (29)$$

where  $\Gamma$  is the incomplete gamma function.

To evaluate equation (29), we take  $\kappa = \epsilon = 1$  (which is consistent with the results of § 6), adopt values of  $t$  and  $r_*$  from equations (26) and (27) (which is appropriate for absorption systems with Ly $\alpha$  equivalent width satisfying  $W > 0.3 \text{ \AA}$ ), adopt  $L_{B_{\min}} = 0.005L_{B_*}$  (which is the minimum galaxy  $B$ -band luminosity at which equation 25 has been established), and consider several recent determinations of the galaxy luminosity function at moderate redshifts. Adopting the galaxy luminosity function of Ellis et al. (1996) (which is characterized by  $\Phi_* = 0.0148_{-0.0019}^{+0.0030} h^3 \text{ Mpc}^{-3}$  and  $s = 1.41_{-0.07}^{+0.12}$  over the redshift interval  $0.15 < z < 0.35$  and includes low surface brightness galaxies), the predicted number density of Ly $\alpha$  absorption systems with  $W > 0.3 \text{ \AA}$  is  $n = 10.4_{-5.3}^{+8.1}$ . Adopting the galaxy luminosity function of Zucca et al. (1997) (which is characterized by  $\Phi_* = 0.020 \pm 0.004 h^3 \text{ Mpc}^{-3}$  and  $s = 1.22_{-0.07}^{+0.06}$  over the redshift interval  $z < 0.3$ ), the predicted number density of Ly $\alpha$  absorption systems with  $W > 0.3 \text{ \AA}$  is  $n = 10.3_{-5.0}^{+6.4}$ . And adopting the galaxy luminosity function of Lilly et al. (1995) (which is characterized by  $\Phi_* = 0.0272 h^3 \text{ Mpc}^{-3}$  and  $s = 1.03$  over the redshift interval  $0.2 < z < 0.5$ ), the predicted number density of Ly $\alpha$  absorption systems with  $W > 0.3 \text{ \AA}$  is  $n = 11.2$ . In comparison, the observed number density of Ly $\alpha$  absorption systems with  $W > 0.3 \text{ \AA}$  is  $n = 21.7 \pm 8.5$  at  $z = 0.35$  (Bahcall et al. 1996). Apparently, luminous galaxies can explain about 50% of Ly $\alpha$  absorption systems with  $W > 0.3 \text{ \AA}$ .

But the predicted number density of Ly $\alpha$  absorption systems depends strongly on the chosen galaxy luminosity function, which inherits two well-known uncertainties: the excess of faint galaxies and the normalization. In addition, the analysis has so far neglected galaxies of luminosity  $L_B < 0.007L_{B_*}$ . If we adopt the galaxy luminosity function of Ellis et al. (1996) over the redshift interval  $0.35 < z < 0.75$  (which is characterized by  $\Phi_* = 0.0355_{-0.0200}^{+0.0291} h^3 \text{ Mpc}^{-3}$  and  $s = 1.45_{-0.18}^{+0.16}$ ), the predicted number density of Ly $\alpha$  absorption systems with  $W > 0.3 \text{ \AA}$  is  $n = 30.6_{-27.4}^{+45.2}$  for  $L_{B_{\min}} = 0.001L_{B_*}$ . If we adopt the modified luminosity function of Zucca et al. (1996) over the redshift interval  $z < 0.3$  (which is characterized by a Schechter form with  $\Phi_* = 0.021 h^3 \text{ Mpc}^{-3}$  and  $s = 1.16$  for  $M_B < -16.99$  and by a power-law form  $(L/L_*)^{-u}$  with  $u = 1.57$  for  $M_B > -16.99$ ), the predicted number density of Ly $\alpha$  absorption systems with  $W > 0.3 \text{ \AA}$  is  $n = 12.9$  for  $L_{B_{\min}} = 0.001L_{B_*}$ . This number is still insufficient to account for all of the observed Ly $\alpha$  absorption systems, but it shows that the faint-end slope of the galaxy luminosity function has a significant influence in the determination of the predicted number density of Ly $\alpha$  absorption systems. We conclude that galaxies might account for all Ly $\alpha$  absorption systems with  $W > 0.3 \text{ \AA}$ , but this depends on the unknown luminosity function and gaseous cross sections of low-luminosity galaxies as well as on the uncertainties of the observed number density of Ly $\alpha$  absorption systems.

## 8. SUMMARY AND CONCLUSIONS

We present initial results of a program to obtain and analyze HST WFPC2 images of galaxies identified in an imaging and spectroscopic survey of faint galaxies in fields of HST spectroscopic

target QSOs. We measure properties of 87 galaxies, of which 33 are associated with corresponding Ly $\alpha$  absorption systems and 24 do not produce corresponding Ly $\alpha$  absorption lines to within sensitive upper limits. Considering only galaxy and absorber pairs that are likely to be physically associated and excluding galaxy and absorber pairs within 3000 km s $^{-1}$  of the background QSOs leaves 26 galaxy and absorber pairs and seven galaxies that do not produce corresponding Ly $\alpha$  absorption lines to within sensitive upper limits. Redshifts of the galaxy and absorber pairs range from 0.0750 to 0.8912 with a median of 0.3718, and impact parameter separations of the galaxy and absorber pairs range from 12.4 to 157.4  $h^{-1}$  kpc with a median of 62.4  $h^{-1}$  kpc. The primary conclusions are as follows:

1. The Ly $\alpha$  absorption equivalent width  $W$  is anti-correlated with galaxy impact parameter  $\rho$  at a level of significance between  $3.36\sigma$  and  $4.45\sigma$ . We conclude that the amount of gas intercepted along the line of sight depends on galaxy impact parameter, which argues that the gas is physically associated with the individual galaxies.

2. The anti-correlation between Ly $\alpha$  absorption equivalent width  $W$  and galaxy impact parameter  $\rho$  accounting for galaxy  $B$ -band luminosity  $L_B$  is superior to the fiducial relationship between  $W$  and  $\rho$ . We conclude that the amount of gas intercepted along the line of sight depends on galaxy  $B$ -band luminosity.

3. The anti-correlation between Ly $\alpha$  absorption equivalent width  $W$  and galaxy impact parameter  $\rho$  accounting for galaxy effective radius  $r_e$  is superior to the fiducial relationship between  $W$  and  $\rho$  but marginally inferior to the relationship between  $W$  and  $\rho$  accounting for  $L_B$ . We conclude that the amount of gas intercepted along the line of sight depends on galaxy effective radius, but only indirectly through the correlation between galaxy effective radius and galaxy  $B$ -band luminosity.

4. The anti-correlation between Ly $\alpha$  absorption equivalent width  $W$  and galaxy impact parameter  $\rho$  accounting for galaxy average surface brightness  $\langle\mu\rangle$ , disk-to-bulge ratio  $D/B$ , or redshift  $z$  is statistically identical to the fiducial relationship between  $W$  and  $\rho$ . We conclude that the amount of gas intercepted along the line of sight does not depend strongly on galaxy average surface brightness, galaxy disk-to-bulge ratio, or redshift. Apparently extended gaseous envelopes are a common and generic feature of galaxies of a wide range of luminosity and morphological type, and Ly $\alpha$  absorption systems trace a significant and representative portion of the galaxy population.

5. The anti-correlation between Ly $\alpha$  absorption equivalent width  $W$  or  $W \cos i$  and galaxy galactocentric radius  $R$  is statistically identical to the fiducial relationship between  $W$  and  $\rho$ . We conclude that spherical halos cannot be distinguished from flattened disks on the basis of the current observations.

6. Most of the galaxies physically associated with Ly $\alpha$  absorbers do not exhibit obvious signs of disturbed morphologies. We conclude that there is no evidence that tenuous gas is distributed around galaxies as a result of galaxy interactions in most cases, although it is of course possible that tenuous gas is distributed around galaxies as a result of galaxy interactions in some cases.

7. Incorporating significant scaling relationships (between  $W$  and  $\rho$  and  $L_B$ ) and rejecting insignificant scaling relationships, our current best estimate of the column density distribution of tenuous gas around galaxies is

$$\log\left(\frac{N}{10^{20} \text{ cm}^{-2}}\right) = -5.33 \log\left(\frac{\rho}{10 \text{ kpc}}\right) - 2.19 \log\left(\frac{L_B}{L_{B*}}\right) + 1.09. \quad (30)$$

The cosmic scatter about this relationship is

$$\sigma_c = 0.815, \quad (31)$$

which corresponds to a factor of  $\approx 6.5$  in neutral hydrogen column density.

8. The relationship between galaxy gaseous radius  $r$  and galaxy  $B$ -band luminosity  $L_B$ , which is analogous to the Holmberg (1975) relationship between galaxy stellar radius and galaxy  $B$ -band luminosity, can be described by

$$\frac{r}{r_*} = \left(\frac{L_B}{L_{B*}}\right)^t, \quad (32)$$

with

$$t = 0.37 \pm 0.11 \quad (33)$$

and

$$r_* = 174^{+38}_{-25} h^{-1} \text{ kpc} \quad (34)$$

for a Ly $\alpha$  absorption equivalent width threshold  $W = 0.3 \text{ \AA}$ . It is clear that  $t = 0$  (no dependence of gaseous radius on galaxy luminosity) can be ruled out at the  $3.4\sigma$  significance level.

9. Applying the relationship between galaxy gaseous radius and galaxy  $B$ -band luminosity to predict the incidence of Ly $\alpha$  absorption systems produced by galaxies drawn from a known galaxy luminosity function, we find that luminous galaxies can explain about 50% of Ly $\alpha$  absorption systems with  $W > 0.3 \text{ \AA}$ . By including lower luminosity galaxies, we find that galaxies might account for all Ly $\alpha$  absorption systems with  $W > 0.3 \text{ \AA}$ . But this depends on the unknown luminosity function and gaseous cross sections of low-luminosity galaxies as well as on the uncertainties of the observed number density of Ly $\alpha$  absorption systems.

The authors thank the staff of STScI for their expert assistance. H.-W.C. and K.M.L. were supported by grant NAG-53261 from NASA; grants GO-0594-80194A, GO-0594-90194A, and GO-0661-20195A from STScI; and grant AST-9624216 from NSF. X.B. was partially supported by the DGES under project PB95-0122 and acknowledges sabbatical support at Cambridge by the DGES under grant PR95-490.

TABLE 1  
JOURNAL OF OBSERVATIONS

Field	$\alpha$	$\delta$	$z_{\text{em}}$	Filter	Exposure	
					Time (s)	Date
0349–1438 .....	03:49:09.5	–14:38:07.0	0.616	F702W	2400	5 Nov 1995
0405–1219 .....	04:05:27.5	–12:19:31.8	0.574	F702W	2400	18 Jan 1996
0850+4400 .....	08:50:13.6	+44:00:29.0	0.513	F702W	3200	7 Feb 1996
1001+2910 .....	10:01:10.7	+29:10:09.0	0.329	F702W	2400	24 Nov 1995
1354+1933 .....	13:54:42.1	+19:33:43.9	0.719	F702W	2400	12 May 1996
1704+6048 .....	17:04:03.5	+60:48:31.1	0.371	F702W	2400	29 Nov 1995

TABLE 2  
JOURNAL OF ARCHIVAL OBSERVATIONS

Field	$\alpha$	$\delta$	$z_{\text{em}}$	Filter	Exposure	
					Time (s)	Date
0454–2203 .....	04:54:02.2	–22:03:56.0	0.534	F702W	1200	6 Feb 1994
1545+2101 .....	15:45:31.1	+21:01:27.5	0.264	F606W	1800	9 Jun 1994
1622+2352 .....	16:22:32.2	+23:52:02.0	0.927	F702W	24000	20 Dec 1994
2135–1446 .....	21:35:01.2	–14:46:27.3	0.200	F606W	2100	14 Aug 1994

TABLE 3  
SUMMARY OF OTHER OBSERVATIONS

Field	Galaxies		Absorbers	
	Number		Number	
	Included	Reference	Included	Reference
0349–1438 .....	5	1	1	2,3
0405–1219 .....	13	3,4	4	3
0454–2203 .....	8	3	3	3
0850+4400 .....	7	3,5	1	2,3,5
1001+2910 .....	2	1	2	2,3
1354+1933 .....	5	1	3	3
1545+2101 .....	4	6	2	3,6
1622+2352 .....	9	7	8	3,7
1704+6048 .....	5	1,8	4	3
2135–1446 .....	7	3	3	3

REFERENCES—(1) Lanzetta et al. 1995; (2) Bahcall et al. 1993; (3) our own observations and analysis, in preparation; (4) Ellingson & Yee 1994; (5) Lanzetta et al. 1997c; (6) Lanzetta et al. 1996; (7) Steidel et al. 1997; (8) Le Brun, Bergeron, & Boissé 1996.

## REFERENCES

- Bahcall, J. N., Bergeron, J., Boksenberg, A., Hartig, G. F., Jannuzi, B. T., Kirhakos, S., Sargent, W. L. W., Savage, B. D., Schneider, D. P., Turnshek, D. A., Weymann, R. J., & Wolfe, A. M. 1993, *ApJS*, 87, 1
- \_\_\_\_\_. 1996, *ApJ*, 457, 19
- Barcons, X., Lanzetta, K. M., & Webb, J. K. 1995, *Nature*, 376, 321
- Bosma, A. 1981, *AJ*, 86, 1825
- Bowen, D. V., Blades, J. C., & Pettini, M. 1996, *ApJ*, 464, 141
- Burstein, D. 1979, *ApJ*, 234, 435
- Coleman, G. D., Wu, C. C., & Weedman, D. W. 1980, *ApJS*, 43, 393
- Ellingson, E. & Yee, H. K. C. 1994, *ApJS*, 92, 33
- Ellis, R. S., Colless, M., Broadhurst, T., Heyl, J., & Glazebrook, K. 1996, *MNRAS*, 280, 235
- Holmberg, E. 1975, in *Galaxies and the Universe*, ed. A. Sandage, M. Sandage, & J. Kristian (Chicago: Univ. Chicago Press), 123
- Krist, J. 1995, in *Astronomical Data Analysis Software and Systems IV*, ASP Conference Series, Vol. 77, ed. R. A. Shaw, H. E. Payne, & J. J. E. Hayes (San Francisco: Astronomical Society of the Pacific), p. 349
- Lanzetta, K. M., Bowen, D. V., Tytler, D., & Webb, J. K. 1995, *ApJ*, 442, 538
- Lanzetta, K. M., Webb, J. K., & Barcons, X. 1995, in *QSO Absorption Lines*, ed. G. Meylan (Berlin: Springer-Verlag), p. 263
- \_\_\_\_\_. 1996, *ApJ*, 456, L17
- \_\_\_\_\_. 1997a, in *Proceedings of the 18th Texas Symposium on Relativistic Astrophysics*, ed. A. Olinto, J. Frieman, & D. Schramm, in press
- \_\_\_\_\_. 1997b, in preparation
- Lanzetta, K. M., Wolfe, A. M., Altan, H., Barcons, X., Chen, H.-W., Fernández-Soto, A., Meyer, D. M., Ortiz-Gil, A., Savaglio, S., Webb, J. K., & Yahata, N. 1997c, *AJ*, in press
- Le Brun, V., Bergeron, J., & Boissé, P. 1996, *A&A*, 306, 691
- Lilly, S. J., Tresse, L., Hammer, F., Crampton, D., & Le Fèvre, O. 1995, *ApJ*, 455, 108
- Morris, S. L., Weymann, R. J., Smith, B. A., Terriale, R. J., Giovanelli, R., & Irwin, M. 1993, *ApJ*, 419, 524
- Schechter, P. 1976, *ApJ*, 203, 297
- Steidel, C. C., Dickinson, M., & Persson, S. E. 1994, *ApJ*, 437, L75
- Steidel, C. C., Dickinson, M., Meyer, D. M., Adelberger, K. L., & Sembach, K. R., 1997, *ApJ*, 480, 568

- Stoche, J. T., Shull, J. M., Penton, S., Donahue, M., & Carilli, C. 1995, *ApJ*, 451, 24
- van Gorkom, J. H., Carilli, C. L., Stoche, J. T., Perlman, E. S., & Shull, J. M. 1996, *AJ*, 112, 1397
- Zucca, E., Zamorani, G., Vettolani, G., Cappi, A., Merighi, R., Mignoli, M., Stirpe, G. M., Macgillivray, H., Collins, C., Balkowski, C., Cayatte, V., Maurogordato, S., Proust, D., Chincarini, G., Guzzo, L., Maccagni, D., Scaramella, R., Blanchard, A., & Ramella, M. 1997, *A&A*, in press

Fig. 1.— Final images of galaxies obtained with HST using WFPC2 with the F606W (for the 1545+2101 and 2135–1446 fields) or F702W (for the other fields) filter. The spatial extent of each image is roughly  $25 h^{-1}$  kpc on a side, and orientation of each image is arbitrary.

Fig. 2.— Logarithm of Ly $\alpha$  rest-frame equivalent width  $W$  vs. logarithm of galaxy impact parameter  $\rho$ . Circles represent early-type elliptical or S0 galaxies, triangles represent early-type spiral galaxies, and squares represent late-type spiral galaxies; small open symbols represent galaxies of luminosity  $L_B < 0.1L_{B^*}$ , small filled symbols represent galaxies of luminosity  $0.1L_{B^*} < L_B < L_{B^*}$ , and large filled symbols represent galaxies of luminosity  $L_B > L_{B^*}$ ; and symbols with arrows indicate  $3\sigma$  upper limits. The cosmic scatter is indicated by the error bar in the upper-right corner.

Fig. 3.— Logarithm of Ly $\alpha$  rest-frame equivalent width  $W$  vs. logarithm of galaxy impact parameter  $\rho$  scaled by galaxy  $B$ -band luminosity. The scaling factor is determined from the analysis described in § 6. Symbols are as in Figure 2, and the cosmic scatter is indicated by the error bar in the upper-right corner.

Fig. 4.— Logarithm of Ly $\alpha$  rest-frame equivalent width  $W$  times cosine of galaxy inclinations angle  $i$  vs. logarithm of galaxy galactocentric radius  $R$ . Symbols are as in Figure 2, and the cosmic scatter is indicated by the error bar in the upper-right corner.

Fig. 5.— Logarithm of neutral hydrogen column density  $N$  vs. logarithm of galaxy impact parameter  $\rho$  scaled by galaxy  $B$ -band luminosity. The scaling factor is determined from the analysis described in § 6. Neutral hydrogen column densities are determined from Ly $\alpha$  rest-frame equivalent widths under the assumption that Doppler parameters are contained in the range  $20 < b < 40$  km s $^{-1}$ . Symbols are as in Figure 2, and the cosmic scatter is indicated by the error bar in the upper-right corner.